Geochemical and thermodynamic modeling of the petrogenesis of A1-type granites and associated intermediate rocks: a case study from the central Fennoscandian Shield

Kärenlampi, Kimmo

2021-05

Kärenlampi , K , Heinonen , J S , Kontinen , A , Hanski , E & Huhma , H 2021 , ' Geochemical and thermodynamic modeling of the petrogenesis of A1-type granites and associated intermediate rocks: a case study from the central Fennoscandian Shield ' , Chemie der Erde , vol. 81 , no. 2 , 125734 . https://doi.org/10.1016/j.chemer.2020.125734

http://hdl.handle.net/10138/333528
https://doi.org/10.1016/j.chemer.2020.125734

Geochemistry - Interdisciplinary Journal for Chemical Problems of the Geosciences and Geoecology xxx (xxxx) xxx

Contents lists available at ScienceDirect

Geochemistry

journal homepage: www.elsevier.com/locate/chemer

Geochemical and thermodynamic modeling of the petrogenesis of A1-type granites and associated intermediate rocks: A case study from the central Fennoscandian Shield

Kimmo Kärenlampi [a,*], Jussi S. Heinonen [b], Asko Kontinen [c], Eero Hanski [a], Hannu Huhma [d]

[a] Oulu Mining School, P.O. Box 3000, 90014 University of Oulu, Finland
[b] Department of Geosciences and Geography, P.O. Box 64, 00014 University of Helsinki, Finland
[c] Geological Survey of Finland, P.O. Box 1237, 70211 Kuopio, Finland
[d] Geological Survey of Finland, P.O. Box 96, 02151 Espoo, Finland

ARTICLE INFO

Handling Editor: Astrid Holzheid

Keywords:
A1-type granite
Ferroan granite
Geochemistry
Sm-Nd isotopes
Magma Chamber Simulator
Paleoproterozoic
Finland
Otanmäki

ABSTRACT

The origin of ferroan A-type granites in anorogenic tectonic settings remains a long-standing petrological puzzle. The proposed models range from extreme fractional crystallization of mantle-derived magmas to partial melting of crustal rocks, or involve combination of both. In this study, we apply whole-rock chemical and Sm-Nd isotopic compositions and thermodynamically constrained modeling (Magma Chamber Simulator, MCS) to decipher the genesis of a suite of A1-type peralkaline to peraluminous granites and associated intermediate rocks (monzodiorite-monzonite, syenite) from the southwestern margin of the Archean Karelia craton, central Finland, Fennoscandian Shield. These plutonic rocks were emplaced at ca. 2.05 Ga during an early stage of the break-up of the Karelia craton along its western margin and show trace element affinities to ocean island basalt-type magmas. The intermediate rocks show positive ε_{Nd}(2050 Ma) values (+1.3 to +2.6), which are only slightly lower than the estimated contemporaneous depleted mantle value (+3.4), but much higher than average ε_{Nd}(2050 Ma) of Archean TTGs (–10) in the surrounding bedrock, indicating that these rocks were essentially derived from a mantle source. The ε_{Nd}(2050 Ma) values of the peralkaline and peraluminous granite samples overlap (–0.9 to +0.6 and –3.2 to +0.9, respectively) and are somewhat lower than those in the intermediate rocks, suggesting that the mafic magmas parental to granite must have assimilated some amount of older Archean continental crust during their fractionation, which is consistent with the continental crust-like trace element signatures of the granite members. The MCS modeling indicates that fractional crystallization of mantle-derived magmas can explain the major element characteristics of the intermediate rocks. The generation of the granites requires further fractional crystallization of these magmas coupled with assimilation of Archean crust. These processes took place in the middle to upper crust (~2–4 kbar, ~7–15 km) and involved crystallization of large amounts of clinopyroxene, plagioclase and olivine. Our results highlight the importance of coupled FC-AFC processes in the petrogenesis of A-type magmas and support the general perception that magmas of A-type ferroan granites become more peraluminous by assimilation of crust. They further suggest that variable fractionation paths of the magmas upon the onset of assimilation may explain the broad variety of A-type felsic and intermediate igneous rocks that is often observed emplaced closely in time and space within the same igneous complex.

1. Introduction

A-type granites are found in various tectonic settings throughout the geological record and have been the subject of extensive research on their petrology, geochronology, geochemistry, and metallogeny (Eby, 1992; Bonin, 2007; Frost and Frost, 2011; Dall'Agnol et al., 2012; Grebennikov, 2014; Dostal, 2016). These granites are typically rich in high-field-strength elements (HFSEs: e.g., Zr, Nb, REE, Y) and low in trace elements compatible in plagioclase and mafic silicates (e.g., Sr, Sc, Co, Ni) (Pearce et al., 1984; Whalen et al., 1987; Eby, 1992; Dall'Agnol et al., 2012). They are characterized by high $FeO_{tot}/(FeO_{tot} + MgO)$ ratios and can be divided into peralkaline, metaluminous, and

* Corresponding author.
E-mail address: kimmo.karenlampi@oulu.fi (K. Kärenlampi).

https://doi.org/10.1016/j.chemer.2020.125734
Received 1 July 2020; Received in revised form 4 November 2020; Accepted 13 December 2020
Available online 28 December 2020

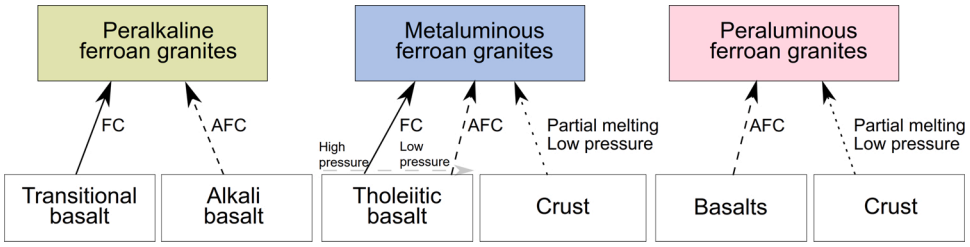

Fig. 1. Schematic summary of the petrogenesis of different types of ferroan A-type granite (modified after Frost and Frost, 2011). Peralkaline ferroan granites form by differentiation of transitional or alkali basalt potentially with some crustal assimilation. Metaluminous ferroan granite may form by differentiation of tholeiitic basalt with or without crustal assimilation and partial melting of quartzo-feldspathic crust at low pressure. Ferroan granites become peraluminous by involvement of partial melts of quartzo-feldspathic crust.

peraluminous granite varieties on the basis of the indexes of alkalinity (molar $Al_2O_3/Na_2O + K_2O$ = A/NK) and aluminosity (molar $Al_2O_3/(CaO + Na_2O + K_2O)$ = A/CNK). The division based on the A/NK and A/CNK indexes has a great petrogenetic importance, as granites that are different in this respect seem to have different origins, even if they were emplaced closely in space and time (e.g., Tommasini et al., 1994; Smith et al., 1999; Shellnut and Zhou, 2007; Donskaya et al., 2018). The three most frequently suggested petrogenetic processes to produce ferroan A-type granite are: 1) partial melting of quartzo-feldspathic crustal rocks, 2) differentiation of tholeiitic or alkali basaltic to transitional basaltic magmas, and 3) a combination of the first two, in which basaltic magmas assimilate crustal rocks (Frost and Frost, 2011). These processes

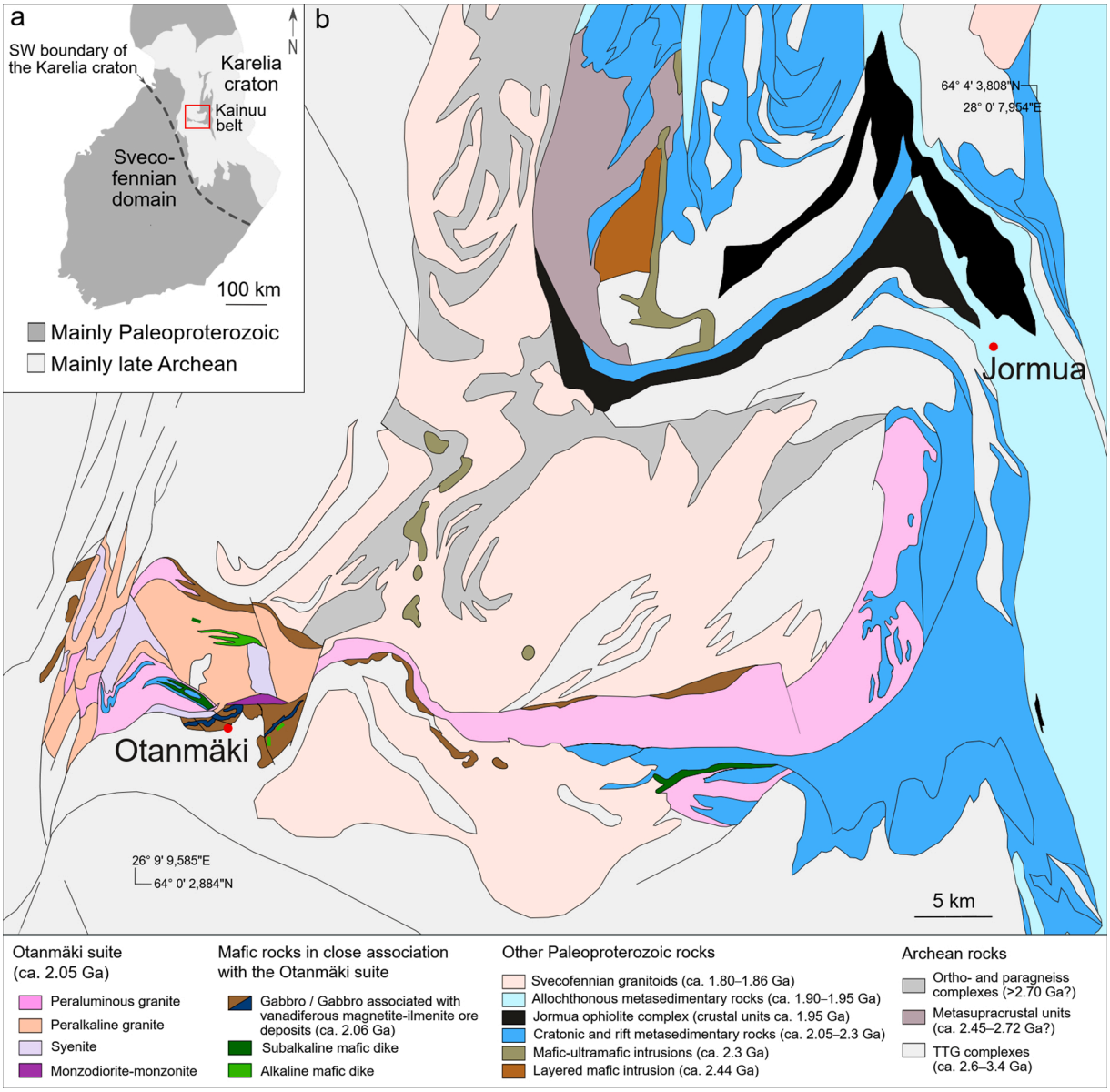

Fig. 2. a) Location of the study area (red rectangle) and the Kainuu belt close to the SW margin of the Archean Karelia craton. b) Map showing the geological setting of the Otanmäki suite A1-type felsic to intermediate igneous rocks on the west side of the Kainuu belt (modified after Bedrock of Finland – DigiKP and Kärenlampi et al., 2019) (For interpretation of the references to colour in this figure legend, the reader is referred to the web version of this article).

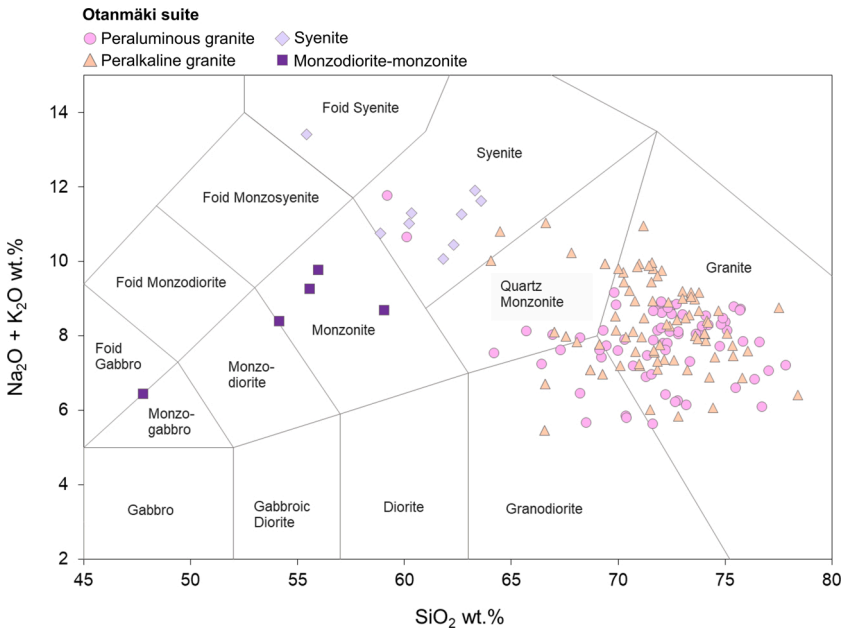

Fig. 3. Total alkali vs. SiO_2 diagram (Middlemost, 1994) for Otanmäki suite felsic and intermediate igneous rocks.

may account for the full range of the observed A-type granite compositions (Fig. 1).

The widespread Svecofennian 1.93–1.77 Ga pre-, syn-, and post-orogenic granitoid magmatism in Finland (Nironen, 2005) was followed by the intrusion of 1.64–1.54 Ga anorogenic A-type rapakivi granites (Rämö et al., 2005). Before 1.93 Ga, the Paleoproterozoic geological evolution involved deposition of sedimentary rocks and mafic and minor felsic volcanic rocks on the Archean basement and emplacement of coeval mafic and rare felsic intrusions (Laajoki, 2005; Iljina and Hanski, 2005; Vuollo and Huhma, 2005; Hanski, 2013; Hanski and Melezhik, 2013a, b). The felsic intrusions are found as relatively small granitic plutons in northern, central and eastern Finland and have ages between 2.4–2.0 Ga (Ahtonen et al., 2007; Mikkola, 2011; Ranta et al., 2015; Kärenlampi et al., 2019). They also include the ca. 2.05 Ga Otanmäki suite in central Finland, which records a rare event of pre-orogenic felsic to intermediate plutonic magmatism at the SW margin of the Archean Karelia craton (Kärenlampi et al., 2019). The main rock types in the Otanmäki suite are peralkaline to peraluminous granite and to some extent associated intermediate rocks, including monzodiorite-monzonite and syenite. These igneous rocks show trace element characteristics similar to those of continental rift-related A1-type granites, which are commonly considered to have formed by differentiation of oceanic island basalt (OIB) -type magmas (Eby, 1992). Unlike the intermediate A1-type rocks of the Otanmäki suite, the granite members show similarity in several incompatible trace element ratios (e.g., Th/Nb, Nb/U, Ce/Nb, and Rb/Nb) to those of Archean TTG gneisses rather than those of OIBs, indicating an important role of the surrounding older crust in their genesis (Kärenlampi et al., 2019).

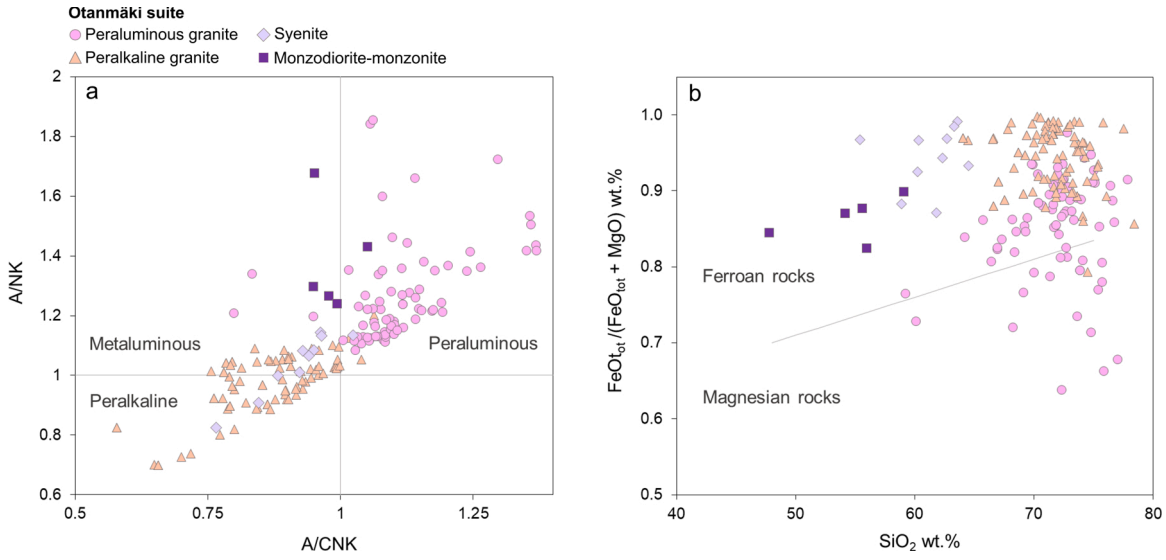

Fig. 4. Major element classification diagrams for Otanmäki suite A1-type felsic and intermediate rocks. a) A/NK (molar $Al_2O_3/(Na_2O + K_2O)$) vs. A/CNK (molar $Al_2O_3/(CaO + Na_2O + K_2O)$) diagram (Shand, 1943). b) $FeO_{tot}/(FeO_{tot}+MgO)$ vs. SiO_2 diagram (Frost and Frost, 2008).

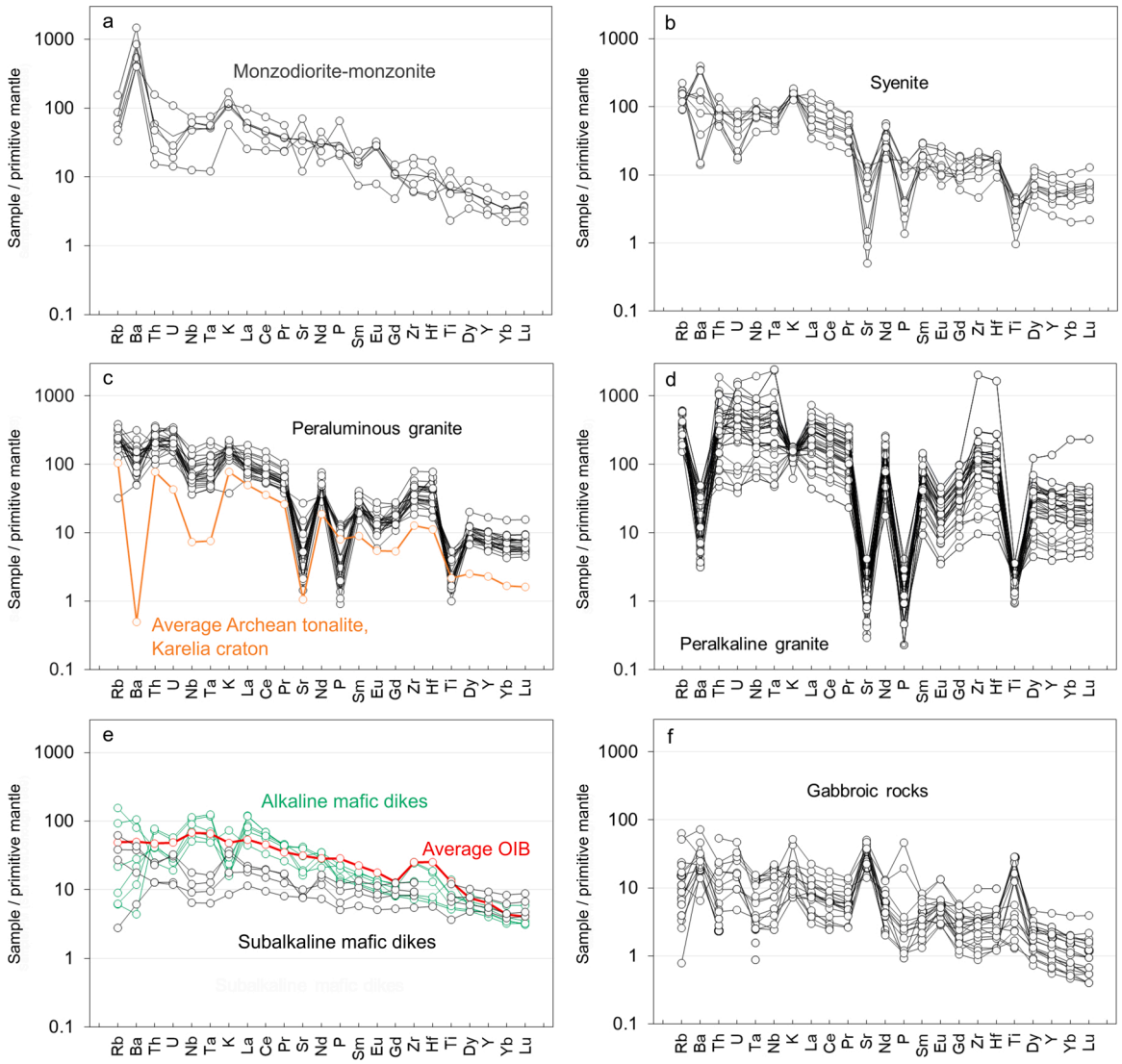

Fig. 5. Primitive mantle-normalized multi-element diagrams for intermediate rocks (a – b) and granite (c – d) from the Otanmäki suite and associated mafic rocks (e – f). Composition of average Archean tonalite from the Karelia craton (Rock geochemical database of Finland, Rasilainen et al., 2007) and average OIB (Sun and McDonough, 1989) are also shown in c) and e), respectively. Normalization values are from Sun and McDonough (1989).

In this study, we present new whole-rock geochemical and Sm-Nd isotope data for samples from the Otanmäki A1-type granite and associated intermediate rocks. These data together with thermodynamically constrained numerical modeling of fractional crystallization and assimilation processes are used to examine the magma sources and petrogenetic processes responsible for the generation of such chemically diverse rock types occurring close together within a single magmatic suite.

2. Geologic setting

The A1-type igneous rocks of the Otanmäki suite are located close to the major collisional boundary between the Paleoproterozoic Svecofennian domain and the Karelia craton (Fig. 2a). The age of the A1-type magmatism has been constrained by U-Pb zircon dating of granitic members, producing ages between 2060 and 2040 Ma, including a precise magmatic age of 2050 ± 2 Ma (Kärenlampi et al., 2019). These results demonstrate that the magmatism took place in an early stage of the break-up that happened along the now western margin of the Karelia craton and eventually led to the development of a continental passive margin and a nascent ocean basin, as witnessed by the 1.95 Ga Jormua ophiolite complex located 20–40 km to the north of the Otanmäki suite A1-type rocks (Peltonen and Kontinen, 2004; Fig. 2b). The craton margin was apparently relatively short lived, as it was soon involved in the Svecofennian protocontinent–continent collisional event, usually inferred to have initiated at ca. 1.90 Ga (Lahtinen et al., 2015). The Otanmäki suite A1-type plutons were affected by the Svecofennian thrusting and subsequent amphibolite-facies (~550–600 °C and ~4 kbar) metamorphism (Kärenlampi et al., 2019). Consequently, the pervasively deformed and gneissic A1-type rocks occur as a lens-shaped, 3 × 8-km-sized body and a 60-km-long, E- to W-trending thrust sheet, both with faulted boundaries against the surrounding Archean TTG complexes and Paleoproterozoic cratonic platformal and riftogenic supracrustal rocks of the adjacent Kainuu belt (Fig. 2b).

The western part of the thrust sheet consists mainly of peralkaline granite and associated syenite and monzodiorite-monzonite, which are mingled with blocks of peraluminous granite (Fig. 2b). Its eastern parts and the lens-shaped body are dominated by peraluminous granite (Fig. 2b). Because of the limited exposure, the available information of the contacts between the various A1-type rocks in the nappes is scanty. Based on aeromagnetic anomaly patterns and field observations, these rocks seem to occur as separate, fault-bound bodies without cutting or mixing relationships, thus making it challenging to constrain their emplacement relationships and depths. However, at least the

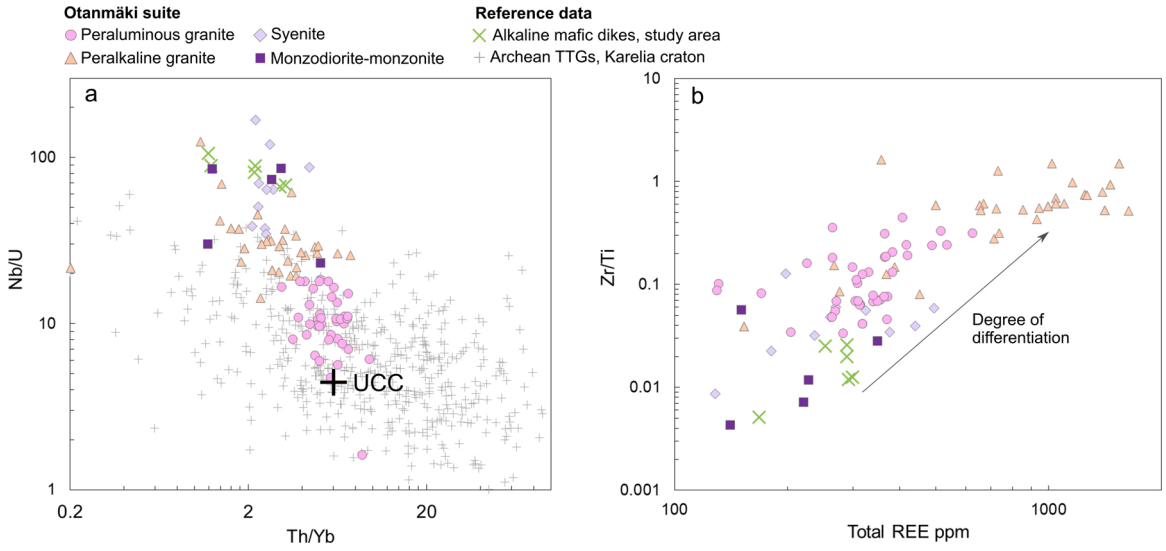

Fig. 6. A1-type rocks and alkaline mafic dikes from the Otanmäki area plotted in a) Nb/U vs. Th/Yb and b) Zr/Ti vs. total REE diagrams. In a) compositions of TTGs in the Karelia craton (Rock geochemical database of Finland; Rasilainen et al., 2007), and average upper continental crust (Rudnick and Gao, 2003) are shown for comparison.

peraluminous granite was probably emplaced at a shallow crustal depth, as it has locally intrusive contact relationships with supracrustal rocks resembling the Paleoproterozoic metasedimentary strata initially deposited on the Karelia craton. At ca. 2.05 Ga, these strata had a maximum thickness of approximately 3–5 km (Laajoki, 2005). The peralkaline granite and associated intermediate rocks sometimes contain mafic enclaves. A striking feature of all of the Otanmäki suite A1-type rocks is that they lack detected intrusive contacts with the surrounding Archean complexes and obvious Archean xenoliths.

Whole-rock zircon saturation temperature estimates calculated using the equation of Boehnke et al. (2013) are about 850–950 °C for the Otanmäki suite granites, which indicates hot peak magmatic temperatures characteristic of A-type granite magmas (e.g., Patiño Douce, 1997; Vilalva and Vlach, 2014). The A1-type rocks show mostly pervasive deformation and recrystallization of their igneous textures and thus likely became re-equilibrated between their minerals during the regional metamorphism, what makes it difficult to judge to what extent, the current minerals of the rocks represent their primary species and compositions. The monzodioritic-monzonitic rocks only occur in one locality where they grade to each other without sharp boundaries. They consist dominantly of calcic plagioclase (~15–40 vol.%), potassium feldspar (~15–35 vol.%) and variable proportions of amphibole (~5–20 vol.%), biotite (~5–20 vol.%), Fe-Ti oxides (~2–5 vol.%), and titanite (~1–5 vol.%). The syenitic rocks have QAP compositions of quartz syenite to alkali feldspar syenite and contain variable amounts of amphibole (~4–12 vol.%), clinopyroxene (~3–15 vol.%), biotite (~0–5%), and magnetite (~0–2%) as mafic minerals. The QAP compositions of the granites range from alkali feldspar granite to monzogranite. The peralkaline granite contains amphibole and/or clinopyroxene (~5–15 vol. % combined), and variable amounts of magnetite (~0–5%) as mafic minerals whereas the peraluminous granite contains variable amounts of biotite (~1–8 vol.%), amphibole (~0–5 vol.%), and magnetite (~0–2

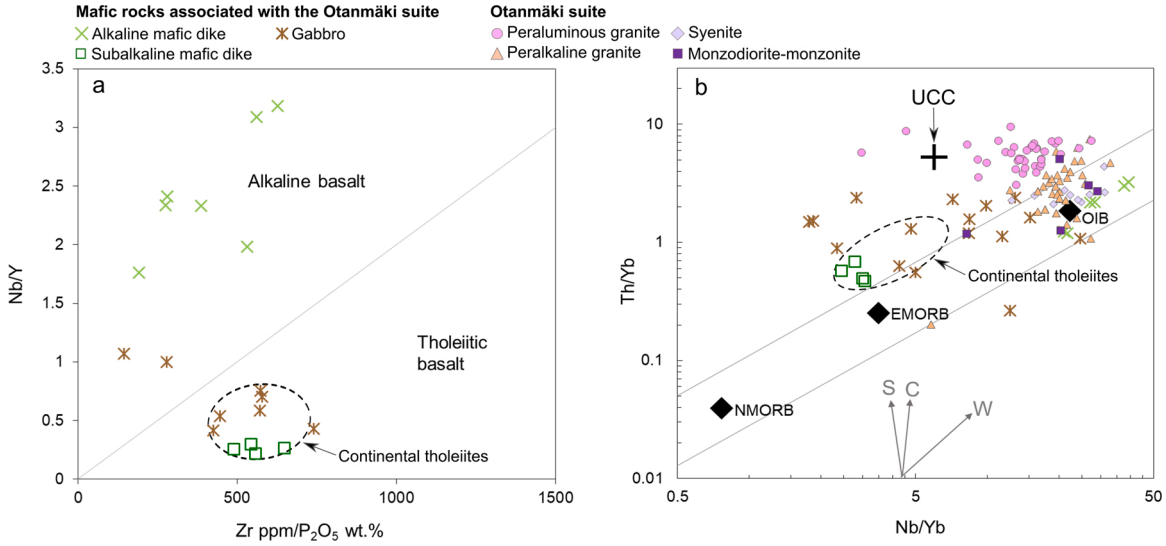

Fig. 7. Trace element ratio diagrams for rocks from the Otanmäki area. a) Nb/Y vs. Zr/P_2O_5 diagram (Floyd and Winchester, 1975). b) Th/Yb vs. Nb/Yb diagram from Pearce (2008) showing the mantle array and average compositions of NMORB (Normal Mid Ocean Ridge Basalt), EMORB (Enriched Mid Ocean Ridge Basalt), and OIB (Ocean Island Basalt). Influence of subduction component (S), crustal contamination (C) and within-plate component (W) indicated by vectors. Also, a field of continental tholeiitic basalts (dashed line) (Farmer, 2003) and average composition of upper continental crust (UCC; Rudnick and Gao, 2003) are shown.

Table 1
Sm-Nd isotope data for samples from the Otanmäki suite A1-type igneous rocks.

Rock type	Northing (WGS84)	Easting (WGS84)	Sample	Analytical method	Nd (ppm)	Sm (ppm)	$^{143}Nd/^{144}Nd$	2SE	$^{147}Sm/^{144}Nd$	ε_{Nd}	$^{143}Nd/^{144}Nd$ (2050 Ma)	ε_{Nd} (2050 Ma)
Monzodiorite	64° 7′ 33,773″	27° 8′ 22,756″	M1	HR-MC-ICP-MS	46	8.3	0.511582	0.000006	0.1085	−20.6	0.510118	2.6 ± 0.1
Monzonite	64° 7′ 30,401″	27° 8′ 37,002″	M2	HR-MC-ICP-MS	33	6.9	0.511767	0.000006	0.1268	−17.0	0.510055	1.3 ± 0.1
Syenite	64° 8′ 17594″	27° 8′ 56,247″	S1	HR-MC-ICP-MS	38	7.0	0.511591	0.000009	0.1095	−20.4	0.510113	2.5 ± 0.2
Syenite	64° 9′ 23094″	26° 55′ 34,299″	S2	HR-MC-ICP-MS	59	9.5	0.511418	0.000014	0.0980	−23.8	0.510096	2.1 ± 0.3
Peralkaline granite	64° 7′ 25,927″	27° 6′ 26,326″	A1149	ID-TIMS	37	6.6	0.51147	0.000020	0.1076	−22.8	0.510017	0.6 ± 0.4
			A1149#2		37	6.6	0.511454	0.000010	0.1071	−23.1	0.510008	0.4 ± 0.2
Peralkaline granite	64° 8′ 30,289″	26° 56′ 33524″	1-OTA	ID-TIMS	105	20	0.511475	0.000011	0.1126	−22.7	0.509956	−0.6 ± 0.2
Peralkaline granite	64° 8′ 50284″	27° 1′ 1,961″	AG1	ICP-SFMS	201	40	0.511548	0.000006	0.1191	−21.3	0.509941	−0.9 ± 0.1
Peralkaline granite	64° 8′ 9,616″	26° 56′ 20,259″	A100	ID-TIMS	100	20	0.511568	0.000010	0.1205	−20.9	0.509942	−0.9 ± 0.2
Peraluminous granite	64° 6′ 54,939″	27° 30′ 14,317″	AG8	HR-MC-ICP-MS	111	17	0.511322	0.000004	0.0956	−25.7	0.510031	0.9 ± 0.1
Peraluminous granite	64° 7′ 55,178″	27° 50′ 46,458″	A1896	ID-TIMS	46	9.7	0.511753	0.000020	0.1283	−17.3	0.510021	0.7 ± 0.4
Peraluminous granite	64° 14′ 43,663″	27° 54′ 8,221″	AG10	HR-MC-ICP-MS	54	9.6	0.511406	0.000007	0.1071	−24.0	0.509961	−0.5 ± 0.1
Peraluminous granite	64° 11′ 20,919″	27° 53′ 51924″	AG7	HR-MC-ICP-MS	55	10.1	0.511454	0.000008	0.1113	−23.1	0.509951	−0.7 ± 0.2
Peraluminous granite	64° 9′ 16,688″	27° 52′ 14,615″	A1832	ID-TIMS	51	9.6	0.511467	0.000020	0.1145	−22.8	0.509922	−1.3 ± 0.4
Peraluminous granite	64° 7′ 49,635″	27° 1′ 23,360″	MG1	HR-MC-ICP-MS	50	8.7	0.511362	0.000005	0.1067	−24.9	0.509922	−1.3 ± 0.1
Peraluminous granite	64° 4′ 13,595″	27° 39′ 47,245″	A1834	ID-TIMS	62	10.7	0.511297	0.000011	0.1032	−26.2	0.509904	−1.6 ± 0.2
Peraluminous granite	64° 4′ 38,706″	27° 40′ 18,460″	A1833	ID-TIMS	90	16	0.511338	0.000016	0.1079	−25.4	0.509882	−2.1 ± 0.3
Peraluminous granite	64° 9′ 4,206″	27° 53′ 16,216″	A989	ID-TIMS	53	9.8	0.511326	0.000020	0.1109	−25.6	0.509829	−3.1 ± 0.4
			A989#2		47	8.5	0.511288	0.000010	0.1091	−26.3	0.509815	−3.4 ± 0.2

The ε_{Nd} (present day) and ε_{Nd} (2050 Ma) values were calculated after DePaolo and Wasserburg (1976) using $\lambda^{147}Sm = 6.54{\cdot}10^{-12}$ a^{-1}, $^{147}Sm/^{144}Nd = 0.1966$ and $^{143}Nd/^{144}Nd = 0.512640$ for the present CHUR. # = duplicated analysis. HR-MC-ICP-MS = high resolution multi collector inductively coupled mass spectrometry, ICP-SFMS = inductively coupled sector field mass spectrometry, ID-TIMS = isotope dilution thermal ionization mass spectrometry.

vol.%).

Mafic intrusive rocks are scarce in the area, although the thrust sheet is locally fringed by tectonized gabbroic bodies. The most prominent of them is the Fe-Ti-V oxide ore-bearing Otanmäki gabbro, which has been dated at 2058 ± 15 Ma (Fig. 2b; Huhma et al., 2018), and is thus roughly coeval with the ca. 2.05 Ga A1-type magmatism. However, the main gabbro bodies and the A1-type rocks are separated by faults, indicating that their current spatial association is due to tectonism. Geochemically, the gabbroic rocks show a continental tholeiite affinity and thus seem to be genetically unconnected to the OIB-affinity A1-type magmatism (see section 4). The gabbros are cut by meter-wide A1-type granite and syenite dikes and both the gabbros and A1-type rocks are cut by subalkaline and alkaline mafic dikes with unknown ages. The alkaline mafic dikes have an OIB-like chemical signature, indicating that they could be petrogenetically linked to the A1-type magmatism.

3. Materials and methods

Whole-rock major and trace element compositions were determined in two laboratories, the Bureau Veritas Minerals Ltd (Canada) and Labtium Oy (Finland). Samples were crushed by a Mn-steel jaw crusher and pulverized using a high-purity carbide steel or a tungsten-carbide-cobalt mill. The analyses at Bureau Veritas were made using inductively coupled plasma optical emission spectrometry and mass spectrometry (ICP-OES/-MS; protocols LF300 and LF100, analytical package LF200), which included sample powder fusion in lithiumborate and dissolution in nitric acid. Total S and C contents were determined using LECO combustion analysis (protocol TC003) and F by a fluoride specific ion electrode (protocols GC840, GC841). The analysis of certified reference materials GSP-2 and SARM-4, which were included in the batches sent to Bureau Veritas, resulted in an excellent correspondence with the certified element concentrations (see Electronic Appendix A). In addition, we report unpublished major and trace element data of alkaline mafic dike samples from the Otanmäki area obtained using a Siemens SRS 303 XRF spectrometer and pressed powder pellets at the University of Oulu and ICP-MS analysis at the Geological Survey of Finland (GTK) following the protocol 308 M (for more details see Rasilainen et al., 2007). In addition to the analytical data mentioned above, we utilized major and trace element analyses from Kärenlampi et al. (2019; 2020) and the Rock Geochemical Database of Finland (Rasilainen et al., 2007). Full list of whole-rock geochemical analyses and analytical methods/protocols used for each sample are given in Electronic Appendix A.

Whole-rock Sm-Nd isotope analyses were performed in three different stages. The compositions of the first sample batch were measured in 2006–2008 at the GTK using isotope dilution thermal

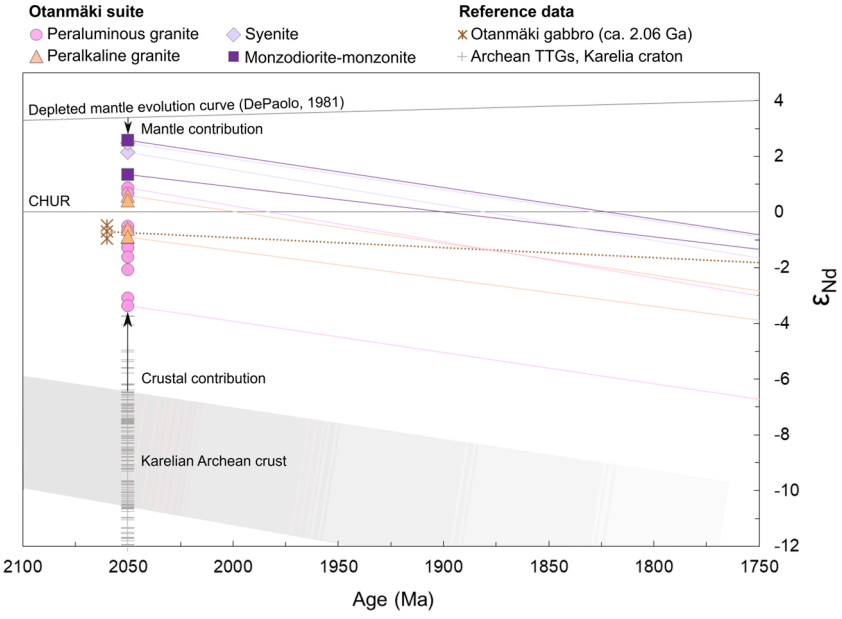

Fig. 8. ε_{Nd} vs. age (Ma) diagram for samples of A1-type peralkaline and peraluminous granite and intermediate igneous rocks from the Otanmäki suite. For comparison, data are also shown for samples from the ca. 2.06 Ga Otanmäki gabbro intrusion (Huhma et al., 2018) and Archean TTGs from the Karelia craton (ε_{Nd} calculated at 2050 Ma, Isotope database of Finland, www.gtk.hakku.fi/en). Depleted mantle evolution curve after DePaolo (1981).

ionization mass spectrometry (ID-TIMS) as described by Huhma et al. (2018). One sample was analyzed in 2018 at ALS Scandinavia AB using inductively coupled plasma-sector field mass spectrometry (ICP-SFMS), following its standard procedure including digestion of samples by alkali fusion and dissolution a $C_4H_6O_6$-HNO_3 mixture and separation of Sm and Nd by ion exchange chromatography. The latest batch was analyzed in 2019 at the Finnish Isotope Geoscience Laboratory at GTK using high resolution multicollector ICP-MS after sample digestion in a HF-HNO_3 mixture and separation of Sm and Nd by ion exchange chromatography. Further details on the ICP-SFMS and HR-MC-ICP-MS analytical procedures and accuracy are given in Electronic Appendix B.

In order to evaluate the petrogenetic relationship between the Otanmäki suite intermediate rocks and granite and potential mafic parental magmas, we performed thermodynamic and geochemical modeling using the Magma Chamber Simulator (MCS) code (Bohrson et al., 2014, 2020 https://mcs.geol.ucsb.edu/). MCS enables the user to study assimilation and fractional crystallization (AFC) processes in a multicomponent-multiphase silicate magma-wall rock system using the MELTS family of models (Ghiorso and Sack, 1995; http://melts.ofm-research.org/) as its engine to derive phase equilibria. Based on thermodynamic data and constraints, MELTS uses variations in temperature, pressure, and volume to replicate the thermodynamic and chemical evolution of a magmatic system undergoing (equilibrium or fractional) crystallization or partial melting. For the FC-AFC runs, we used the rhyolite-MELTS version 1.1.0 as the thermodynamic engine of MCS because it has been optimized for silicic systems that saturate in quartz and crystallize to the two-feldspar-, quartz-, fluid-saturated ternary minimum within the SiO_2-TiO_2-Al_2O_3-Fe_2O_3-Cr_2O_3-FeO-MnO-MgO-NiO-CoO-CaO-Na_2O-K_2O-P_2O_5-H_2O compositional space (Gualda et al., 2012; Ghiorso and Gualda, 2015).

In the MCS software, the user can adjust input parameters, such as the magma and wall rock composition, oxidation state, and pressure.

Table 2
Trace element partition coefficients used in the AFC models.

Phase	olivine	orthopyroxene	clinopyroxene	plagioclase	alkali feldspar	spinel	rhombohedral oxide	apatite	biotite	quartz	garnet
Constant values#											
K_{sm}(Nb)	0.001[a]				0.15[b]			0.0024[h]	4.6[b]	0	0.03[i]
K_{sm}(Nd)	0.002[a]				0.51[e]			5.68[h]	0.08[e]	0	0.4[j]
K_{sm}(U)	0.003[a]				0.07[f]			0.17[h]	1.2[f]	0	0.029[i]
High-T (T_1 = 1200 °C) values*											
K_{sm}(Nb)	0.001[a]	0.0013[a]	0.008[a]	0.03[a]		0.01[a]	2.3[a]				
K_{sm}(Nd)	0.002[a]	0.0056[a]	0.1873[a]	0.068[a]		0.0006[a]	0.0012[a]				
K_{sm}(U)	0.003[a]	0.009[a]	0.0028[a]	0.05[a]		0.001[a]	0.09[a]				
Low-T (T_2 = 700 °C) values*											
K_{sm}(Nb)		0.73[b]	1[b]	0.88[b]		0.18[c]	89.1[b]				
K_{sm}(Nd)		0.6[d]	1.4[d]	0.19[d]		0.93[d]	7.6[f]				
K_{sm}(U)		0.17[f]	0.458[g]	0.13[f]		0.83[f]	3.2[f]				

#Constant values are used for phases that only appear in high (ol) or low (ksp, apa, biot, qtz) temperatures. *Temperature-dependent values are used for phases that appear under wide range of temperatures. At any given T, K_{sm} is calculated by the equation $K_{sm}(T) = e\hat{}((A + BT)/T)$, where $A = (T_1T_2\ln(K_2/K_1))/T_1\text{-}T_2$ and $B = \ln K_2\text{-}A/T_2$. Sources for the partition coefficients: [a]Jean Bedard's K_{sm} values from PELE software (version 7.03 (2010); see Boudreau, 1999), [b]Ewart and Griffin (1994; maximum values for low-Si rhyolite), [c]Nielsen and Beard (2000), [d]Bacon and Druitt (1988), [e]Bea et al. (1994), [f]Nash and Crecraft (1985), [g]Mahood and Hildreth (1983; average), [h]Prowatke and Klemme (2006; sample 61A; Nd after Sm), [i]van Westrenen et al. (1999), [j]Sisson and Bacon (1992). All elements are considered incompatible in the WR fluid ($K_{s/H2O}$ is 1000).

Table 3
Whole-rock analyses of OIB-like alkaline mafic dikes and Archean tonalite used as proxies for parental magma and wall rock compositions in the FC-AFC models.

Sample	VUO97/75.80	VUO97/89.10		VUO97/6.40	VUO97/9.45		MHR-90694
Major oxides (wt. %)	**OIB-like mafic dike (Type I)**	**OIB-like mafic dike (Type I)**	**Type I Average**	**OIB-like mafic dike (Type II)**	**OIB-like mafic dike (Type II)**	**Type II Average**	**Tonalite**
SiO_2	45.6	43.5	44.5	46.0	45.7	45.9	71.6
TiO_2	1.20	1.12	1.2	1.80	1.80	1.8	0.32
Al_2O_3	14.34	12.90	13.6	15.01	15.07	15.0	15.10
FeO_{tot}	7.27	9.61	8.4	9.19	9.20	9.2	2.26
MnO	0.13	0.15	0.1	0.13	0.13	0.1	0.04
MgO	8.57	11.22	9.9	7.23	7.57	7.4	0.94
CaO	14.92	13.50	14.2	10.94	11.28	11.1	2.24
Na_2O	2.02	1.30	1.7	3.08	2.88	3.0	5.10
K_2O	0.48	0.71	0.6	0.49	0.53	0.5	1.81
P_2O_5	0.32	0.29	0.3	0.43	0.50	0.5	0.10
Molar Mg/(Mg + total Fe)	68	68	68	58	59	59	–
Trace elements (ppm)							
Rb	5.7	14	9.7	3.9	4.0	3.9	51
Sr	849	342	595	894	652	773	302
Ba	152	198	175	31	83	57	697
Nb	50	43	46	76	82	79	3.9
Ta	2.5	2.2	2.3	4.9	5.1	5.0	0.3
Th	3.9	3.5	3.7	6.3	6.5	6.4	6.9
U	0.6	0.5	0.5	1.1	1.2	1.2	1.3
Zr	90	81	85	272	280	276	145
Hf	2.1	2.0	2.0	5.5	5.8	5.7	3.8
Y	21	18	20	24	26	25	4.6
La	83	81	82	48	59	54	23
Ce	123	122	123	101	114	108	43
Pr	12	12	12	11	13	12	4.3
Nd	39	38	39	42	47	45	14
Sm	5.3	5.1	5.2	7.2	7.7	7.4	2.1
Eu	1.7	1.6	1.6	2.1	2.4	2.2	0.5
Gd	4.9	4.8	4.8	6.4	7.1	6.7	1.6
Tb	0.7	0.7	0.7	0.9	1.0	1.0	0.2
Dy	3.8	3.5	3.7	4.7	4.9	4.8	0.8
Ho	0.7	0.7	0.7	0.8	0.9	0.8	0.2
Er	1.8	1.9	1.8	2.2	2.4	2.3	0.4
Tm	0.3	0.3	0.3	0.3	0.4	0.3	0.05
Yb	1.8	1.6	1.7	1.9	2.2	2.0	0.4
Lu	0.2	0.2	0.2	0.3	0.3	0.3	0.06

Table 4
Parental magma and tonalite wall rock compositions and used in the FC-AFC models and typical wall rock partial melt compositions generated in the AFC models.

Major oxides (wt.%)	Type I parental magma	Type II parental magma	Tonalite wall rock	Wall rock partial melt (708 °C, 2.5 kbar, ~10 % melting)	Wall rock partial melt (754 °C, 2.5 kbar, ~30 % melting)
SiO_2	47.6	48.3	69.7	65.7	71.2
TiO_2	1.24	1.90	0.31	0.14	0.16
Al_2O_3	15.33	15.85	14.70	17.9	12.7
Fe_2O_3	1.50	1.61	1.22	0.14	0.32
FeO	7.02	8.23	1.10	0.42	0.58
MnO	0.15	0.14	0.04	0.41	0.06
MgO	10.58	7.80	0.92	0.11	0.24
CaO	13.54	11.71	2.18	1.78	0.97
Na_2O	1.78	3.14	4.96	1.44	3.88
K_2O	0.64	0.54	1.76	4.82	3.34
P_2O_5	0.33	0.50	0.10	1.22	0.14
H_2O	0.27	0.26	3.01	5.85	6.42
Molar Mg/(Mg + Fe_{tot})	69	59	–	–	–
FeO_{tot}/(FeO_{tot}+MgO) wt.%	0.44	0.55	0.71	0.83	0.79
Molar Al_2O_3/(Na_2O + K_2O)	4.24	2.76	1.46	2.36	1.27
Molar Al_2O_3/(CaO + Na_2O + K_2O)	0.96	0.97	1.22	1.95	1.17
Trace elements (ppm)					
Nb	46	79	3.9	4.3	5.4
Nd	39	45	14	61.6	31.7
U	0.6	1.2	1.3	6.1	2.8
Nd isotopic composition					
$^{143}Nd/^{144}Nd$ (2050 Ma)	0.51012	0.510118	0.509441	0.509441	0.509441
ε_{Nd} (2050 Ma)	2.6	2.6	−10.7	−10.7	−10.7

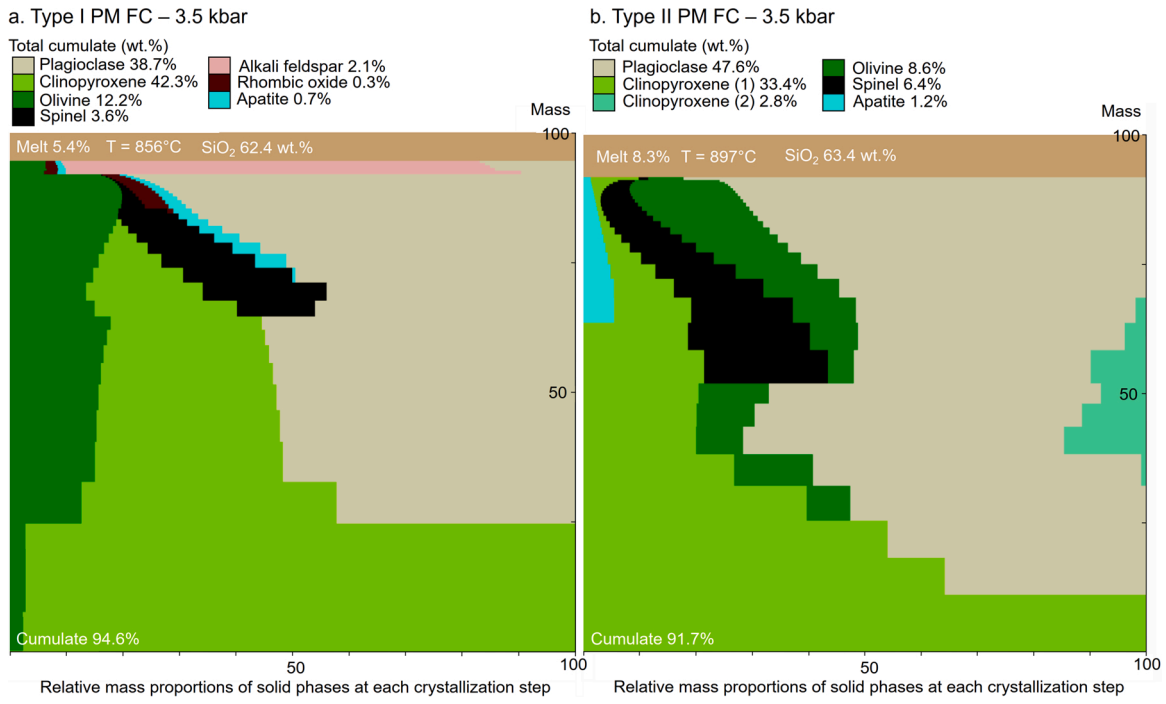

Fig. 9. Cumulate sequences at the end of representative Magma Chamber Simulator (MCS) fractional crystallization (FC) model using type I (a) and type II (b) parental magma (PM) compositions. Model evolution is bottom-up (i.e., earliest cumulates at the bottom, final residual melt at the top). Note that the percentages and the relative proportions reflect mass and not area or volume. SiO_2 content and temperature of the residual melt are also indicated. Figures were created using the MCS Visualizer Tool available from the MCS website (https://mcs.geol.ucsb.edu/).

The FC runs proceed by small individual equilibrium crystallization steps within the input temperature range. At the end of each temperature step, all equilibrium solids are removed from the melt to form cumulates. In AFC runs, the parental magma evolves through FC until the solidus temperature and a user-defined melt percolation threshold of the wall rock have been exceeded and wall rock partial melts are introduced into the magma body and homogenized with the resident magma. Partial melting changes the wall rock modal and chemical compositions as the melting proceeds and the changes are updated accordingly. The fractionation and assimilation steps follow until the run ends based on a user-set target temperature or mass constraint or when thermal equilibrium between the resident magma and wall rock is attained. Trace element and isotope models are implemented after the evolution of phase equilibria and major elements have been constrained (Heinonen et al., 2020). The trace element calculations follow melt-solid-fluid equations (Spera et al., 2007) in each crystallization step using phase-specific partition coefficients for trace elements.

4. Geochemistry

In the Otanmäki A1-type suite, the SiO_2 content varies widely, being ~48 to 55 wt.% in monzodiorite-monzonites, ~60 to 63 wt.% in syenites, and ~68 to 75 wt.% in granites (Fig. 3). In the TAS diagram (Fig. 3), the intermediate rocks (monzodiorite-monzonite, syenite,) define a trend that extends from the field of monzogabbro to that of syenite, while the granites plot dominantly in the field of granite. The A/NK vs. A/CNK diagram (Fig. 4a) classifies the intermediate rocks mostly as metaluminous. The granitic rocks show a division into peralkaline and peraluminous groups, although among the peralkaline granite bodies, the rock compositions locally grade to metaluminous. In the $FeO_{tot}/(FeO_{tot} + MgO)$ vs. SiO_2 diagram (Fig. 4b), the A1-type rocks show dominantly ferroan compositions.

In multi-element primitive mantle-normalized diagrams (Fig. 5), the Otanmäki suite granitic and intermediate rocks all display as groups fairly uniform patterns, suggesting dominantly primary magmatic compositions (see also Kärenlampi et al., 2019), although some mobile elements such as Rb, Ba, K, U, and Th probably show some variation influenced by secondary processes. The monzodiorite-monzonite samples (Fig. 5a) exhibit patterns that are similar to those of average OIB and the OIB-like mafic dikes from the study area (Fig. 5e), with the exception that they are more enriched in Ba, K, and Eu (Eu/Eu* = ~1.3–2.4). The syenite samples show Ti and P depletions and positive K anomalies (Fig. 5b). In terms of trace element characteristics, they can be divided into Ba-Sr-Eu-enriched and -depleted types (relative to REEs, excluding Eu; Fig. 5b), with the former showing positive (Eu/Eu* = ~1.0–3.1) and the latter negative Eu-anomalies (Eu/Eu* = ~0.4–0.9). The granites are characterized by strong depletion in Ba, Sr, P and Ti, enrichment in Zr-Hf relative to REEs (expect Eu), and negative Eu anomalies (Eu/Eu* = ~0.3–0.5 for samples of peralkaline and ~0.6–0.8 for peraluminous granite) (Figs. 5c–d). The trace element patterns also reveal that, compared to the peralkaline granites, the peraluminous granites have significantly lower levels of Nb-Ta relative to Th-U and Zr-Hf, which may be an indication of a greater amount of crustal contamination, as these features are similar to those of the average Archean tonalite from the Karelia craton (Fig. 5c). Furthermore, the peraluminous granite and, to a lesser extent, the peralkaline granite samples show incompatible trace element ratios, such as Nb/U and Th/Yb (Fig. 6a), that are more similar to those of average upper continental crust and Archean TTGs from the Karelia craton, than those of intermediate A1-type rocks and average OIB or alkaline mafic dikes from the Otanmäki area. On the other hand, the peralkaline granites appear more differentiated compared to peraluminous granites and intermediate rocks based on their high Zr/Ti ratios and total REE contents (Fig. 6b).

The mafic rocks associated with the Otanmäki suite are divided into subalkaline and alkaline groups on the Zr/P_2O_5 vs. Nb/Y diagram (Fig. 7a). The fringing gabbroic bodies and the majority of the mafic dikes from the study area are classified as subalkaline, whereas the OIB-like dikes plot in the alkaline field. In multi-element diagrams (Figs. 5e–f), the rocks of the subalkaline group show negative Nb-Ta

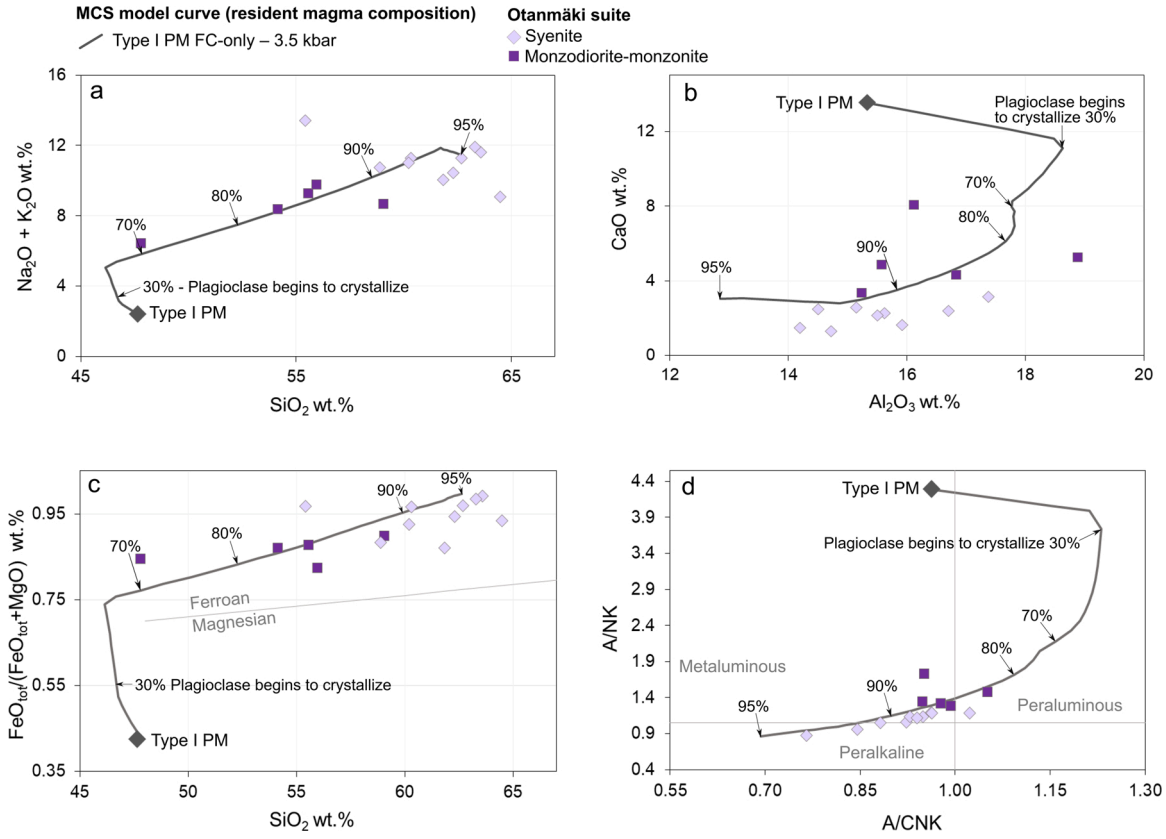

Fig. 10. Major element evolution of the resident magma in Magma Chamber Simulator (MCS) fractional crystallization (FC) model using the type I parental magma (PM) composition compared to Otanmäki suite intermediate igneous rocks in a) total alkali vs. SiO_2, b) CaO vs. Al_2O_3, c) $FeO_{tot}/(FeO_{tot}+MgO)$ vs. SiO_2, and d) A/NK vs. A/CNK diagrams. The degree of crystallization relative to the mass of the parental melt in selected crystallization steps and initiation of plagioclase crystallization is also indicated.

anomalies relative to Th-U, Zr-Hf, and REEs (except Eu), which may indicate crustal contamination. In the Nb/Yb vs Th/Yb diagram (Fig. 7b), the rocks of the subalkaline group are most similar to continental tholeiitic basalts with E-MORB affinities, although the gabbros show relatively large scatter, probably due to secondary alteration related to regional metamorphism. The alkaline mafic dikes plot close to average OIB (Fig. 7b) and the Otanmäki suite A1-type rocks, and their trace element signature does not exhibit any obvious signs of crustal assimilation (Fig. 5e).

5. Sm-Nd isotope results

In order to evaluate the source characteristics of the Otanmäki suite A-type rocks, 17 whole-rock samples were analyzed for Sm-Nd isotopes, many of them being the same as used for U-Pb zircon dating by Kärenlampi et al. (2019). The analytical method used for each sample is shown in Table 1. For comparative purposes, we also utilized Sm-Nd isotope data reported by Huhma et al. (2018) for the 2.06 Ga Otanmäki gabbros (n = 3) and data retrieved from the Isotope database of Finland (www.gtk.hakku.fi/en) for the late Archean TTGs (n = 170) in eastern Finland (see also Huhma et al., 2012).

The samples from the Otanmäki A-type suite have relatively high LREE contents and their initial ε_{Nd} values(2050 Ma) range from –3.4 to +2.6 (Table 1). The intermediate rock samples (monzodiorite, monzonite, syenite) show positive values (+2.6 to +1.3), which are slightly lower than the estimated value for the concurrent depleted mantle (+3.4; DePaolo, 1981) but higher than the values of the gabbro samples in the study area (–0.5 to –0.3 at 2060 Ma) and much higher than ε_{Nd}(2050 Ma) of Archean TTGs in the surrounding bedrock (average –10) (Fig. 8). This indicates that the intermediate rocks were derived essentially from a mantle source rather than from some older fractionated crustal materials. The ε_{Nd}(2050 Ma) values of the granites (–3.2 to +0.9) are, within error limits, lower than those of the intermediate rocks (Table 1; Fig. 8). This suggests that the granites record a larger degree of material contribution from older felsic crust, which is also consistent with their trace element characteristics (Fig. 8). Although peralkaline (–0.9 to +0.6) and peraluminous granites (–3.2 to +0.9) overlap in their ε_{Nd}(2050 Ma) values, in general, the peraluminous granitic rocks are characterized by less radiogenic, i.e., more crustal Nd isotope compositions.

6. Thermodynamic modeling of fractional crystallization and assimilation

Based on the observations made above, FC (fractional crystallization) and AFC (assimilation-fractional crystallization) processes involving mantle-derived parental magma and Archean felsic crust seem to provide a potential mechanism to generate the Otanmäki suite A1-type intermediate and felsic igneous rocks. To evaluate it quantitatively, we conducted numerical modeling of FC and AFC processes using MCS. We performed multiple MCS models to iterate for the best-fit input parameters. The whole MCS output data and related illustrations can be collected from the Electronic Appendix C and only the most successful models are illustrated and discussed below.

6.1. Modeling procedure

The MCS software was used to study the influence of variable input parameters (e.g., initial composition and relative mass of magma and wall rock, degree of critical melt fraction in wall rock, temperature,

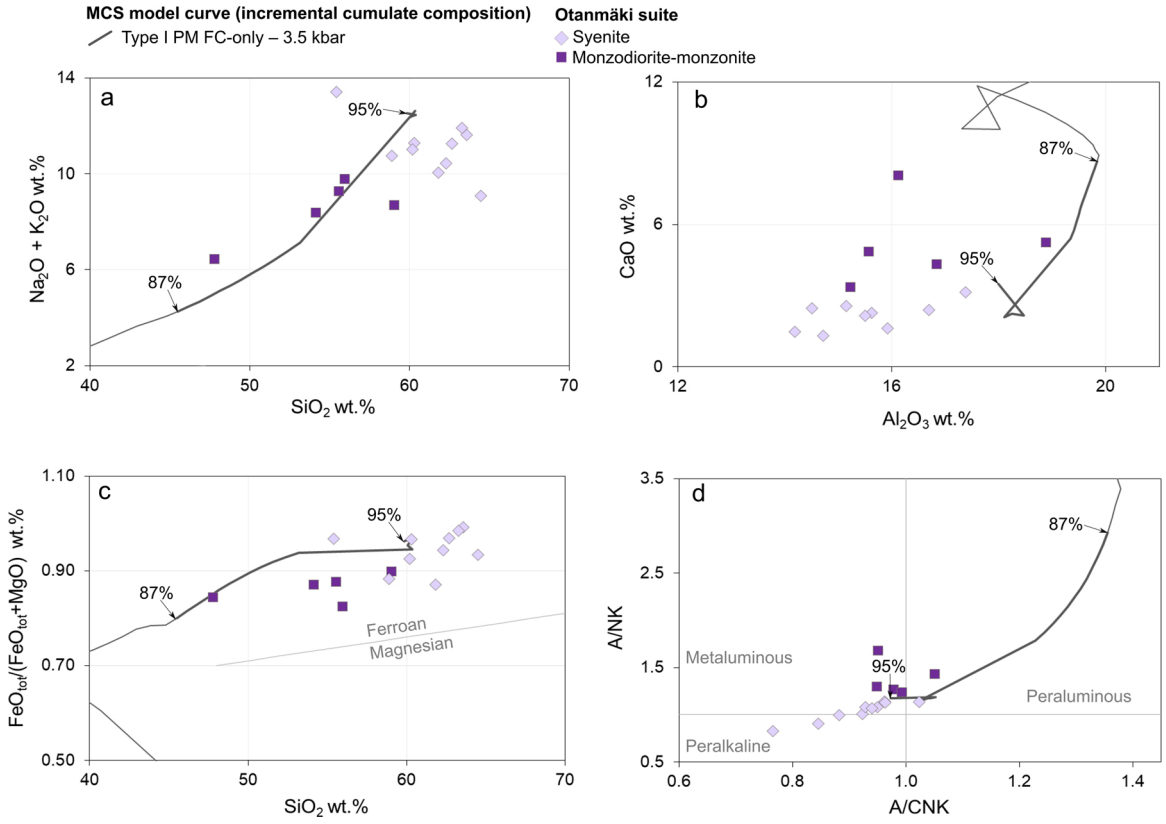

Fig. 11. Major element evolution of incremental cumulates in Magma Chamber Simulator (MCS) fractional crystallization (FC) model using the type I parental magma (PM) composition compared to Otanmäki suite intermediate igneous rocks in a) total alkali vs. SiO_2, b) CaO vs. Al_2O_3, c) $FeO_{tot}/(FeO_{tot}+MgO)$ vs. SiO_2, and d) A/NK vs. A/CNK diagrams. The degree of crystallization relative to the mass of the parental melt in selected crystallization steps is also indicated.

pressure, etc.) and to iterate to find parameters that yield melt compositions and liquid lines of descent most similar to the igneous rocks of the Otanmäki suite. We carried out both FC only and AFC runs. Partition coefficients were compiled based on listings in the EarthRef database (https://earthref.org/KDD/) and are given in Table 2. The output information recorded by the MCS includes the major and trace element and isotope evolution of melt and crystals in the resident magma, wall rock and cumulates.

6.2. Parental melt composition

For the parental melt composition, we tested various mafic compositions ranging from those found in the study area to Fe-tholeiitic and OIB-like melts from the literature (see Electronic Appendix D). Based on this testing, the 1−4-m-wide, OIB-like alkaline mafic dikes that cut the ca. 2.06 Ga Otanmäki gabbro intrusion emerged as the most relevant option. On the basis of whole-rock compositions, two distinct types (I and II) are recognized. Their main difference is that type I has a higher Mg-number and MgO and CaO contents and lower TiO_2, Al_2O_3, Na_2O, P_2O_5, Nb, and Zr contents than type II, indicating that the former represents a more primitive composition (Table 3). In terms of trace element characteristics, both types appear to represent a homogenous group (e.g., Fig. 5e), suggesting that the dikes may be representative of primary melt compositions. Nevertheless, the dikes are metamorphosed and the type I dikes consist of fine-grained, equigranular amphibole and plagioclase, whereas the type II dikes show porphyritic texture and contain recrystallized phenocrysts of plagioclase set in a fine-grained groundmass of plagioclase and amphibole.

As parental melt major and trace element composition, we used average compositions of both the type I and II dikes, in both cases based on two available analyses (Table 4 and Electronic Appendix A). The average composition obtained of the type I dike analyses resulted in stability issues in MELTS and premature halting of the runs. MELTS is sensitive to the input parental melt composition and conditions where suitable phase stability data are limitedly available and therefore it may not always be able to find a reasonable solution. Through extensive testing, we found that only slight adjustments of the SiO_2, CaO, Al_2O_3, Fe_2O_3 and FeO_{tot} contents of the average type I composition resulted in more stable runs and thus this modified composition was used as the type I parental melt composition (Table 4). The Nd isotope composition of the OIB-like mafic dikes is not known, but we used the data obtained from the monzodiorite sample (M1) that has the highest initial ε_{Nd} (2050 Ma) among the A1-type rocks (Table 1). The original oxidation state of iron is also not known, but we assumed a commonly used $FeO/FeO_{tot} = 0.85$ as the initial oxidation state in all runs. Preliminary testing indicated that varying the initial Fe oxidation state had only a negligible effect on the outcome of the FC and AFC calculations.

Another unknown parameter of the parental melt composition is the H_2O content and therefore models were run at varying initial H_2O contents within the typical of OIB range (~0.3–1.5 wt.%; Wallace, 1998; Simons et al., 2002; Dixon and Clague, 2001; Dixon et al., 2002; Weis et al., 2015). The most stable runs were achieved using ~0.3 wt.% H_2O, which also provided the best-fits and was generally used (Table 4). Preliminary modeling showed that increasing the initial H_2O content reduces the stability of plagioclase and produces more aluminous resident magma compositions than the runs with less initial H_2O. Preliminary modeling also showed that increasing the initial H_2O content reduces the stability of plagioclase and produces more aluminous resident magma compositions compared to the runs with less initial H_2O. One unfortunate limitation of rhyolite-MELTS is that it lacks proper thermodynamic models for hydrous mafic phases and hence its poor applicability to mafic-intermediate compositions with abundant hornblende or biotite (see Gualda et al., 2012; Bohrson et al., 2020). Nevertheless, we consider this to be only of minor importance to the

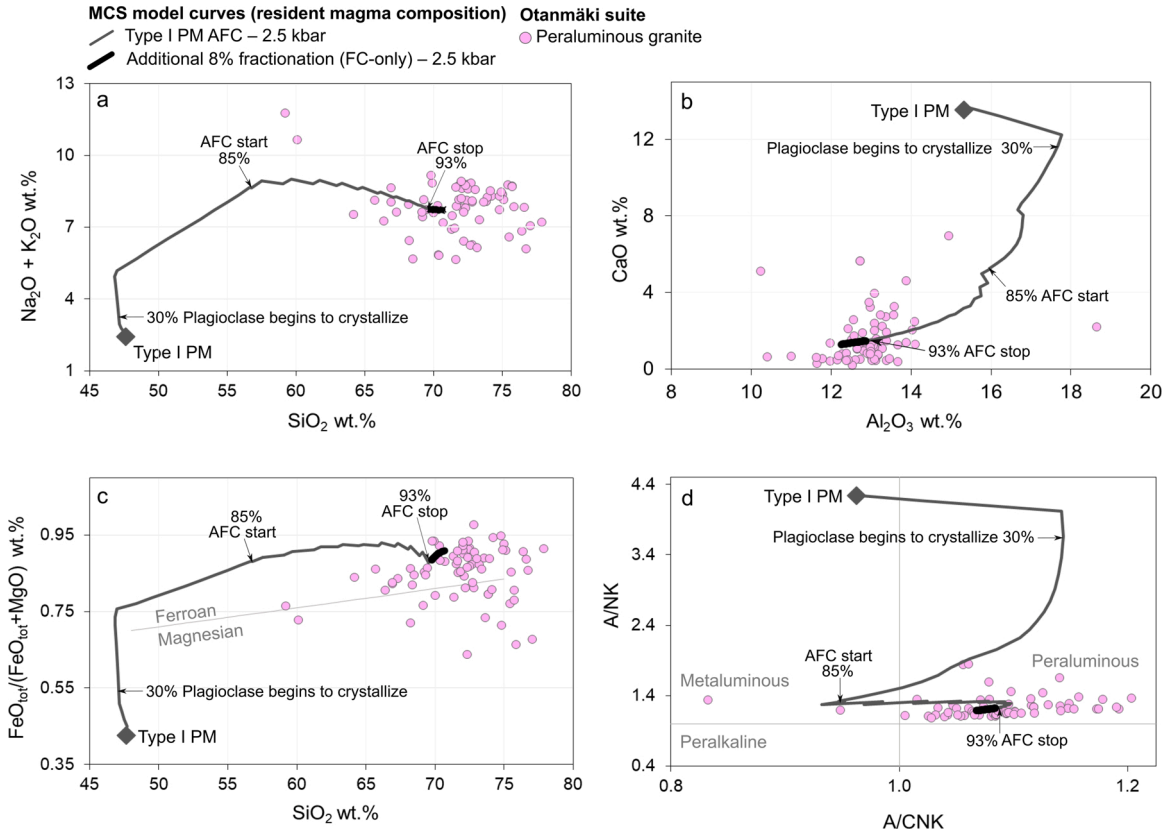

Fig. 12. Major element evolution of resident magma in Magma Chamber Simulator (MCS) assimilation fractional crystallization (AFC) model using the type I parental magma (PM) composition and tonalite wall rock compared to Otanmäki suite peraluminous granite in a) total alkali vs. SiO_2, b) CaO vs. Al_2O_3, c) FeO_{tot}/(FeO_{tot}+MgO) vs. SiO_2, and d) A/NK vs. A/CNK diagrams. Also shown is the resident magma composition produced by additional fractionation of the final melt generated by the AFC model. The degree of crystallization relative to the mass of the parental melt in selected crystallization steps, initiation of plagioclase crystallization and points where assimilation begins and stops is also indicated.

presented models. Amphibole, for example, is not expected to stabilize during crystallization of basaltic magma unless it has very high water contents (>5 wt.% H_2O; see Bonechi et al., 2017), a condition more likely in arc basaltic magmas (e.g., Ushioda et al., 2014) than in OIBs. Furthermore, significant amphibole fractionation produces magma series with some distinct geochemical trends, such as decreasing Dy/Yb and Dy/Dy* ratios with increasing SiO_2 (Davidson et al., 2013). The absence of such trends in the Otanmäki suite suggests amphibole fractionation was not an important process in its generation. The syenitic and granitic rocks in the Otanmäki suite contain abundant amphibole, but it is likely mostly metamorphic in origin as it is often associated with cores of clinopyroxene or occurs as replacement growth zones over clinopyroxene. Also, neither does the presence of abundant amphibole and/or biotite in the granites necessarily mean that these minerals would be fractionated phases as they can also result from crystallization of residual melts and/or subsolidus hydration of anhydrous primary minerals (e.g., Mücke, 2003; Beard et al., 2003; Bucher and Frost, 2006).

6.3. Assimilant composition

Based on the age and trace elements characteristics of the Otanmäki suite granite members and the fact that their host nappes occur interleaved between Archean TTG gneiss complexes, the most plausible assimilant is material from the Archean crust. Therefore, we selected potential assimilant compositions reported for basement rocks of the Karelia craton (Rasilainen et al., 2007; Rock Geochemical database of Finland; www.gtk.hakku.fi/en). We performed iterative test runs using compositions of several relevant TTG-series rocks and found that a tonalite sample from the study area (see Tables 3 and 4 and Electronic Appendix A) provides the best fit. The Nd isotope composition of this tonalite sample is not known, but we used an average $^{143}Nd/^{144}Nd$ ratio for tonalites from the Karelia craton (Table 4; Isotope Database of Finland; www.gtk.hakku.fi/en). As in the case of the parental melt, the oxidation state of Fe and the H_2O content of the wall rocks are not known. For FeO/FeO_{tot} we used 0.5 as the initial ratio. Test runs showed that varying the wall rock oxidation state has a minimal effect on the modeling outcomes. For the wall rock, we tested initial H_2O contents of 1 and 3 wt.%, as the latter provided the best-fits in the AFC models, it was generally used (Table 4). Adding H_2O lowers the solidus temperature of the wall rock significantly, allowing a larger melt fraction to form at lower wall rock temperatures and a larger range of contamination in the models. Preliminary modeling indicated no significant differences in the outcomes if water content of the wall rock was higher than 3 wt.%.

6.4. Pressure, temperature and mass constraints

We ran preliminary models at various pressures (1–6 kbar) with the outcome that the best-fit models for the compositional trends observed in the Otanmäki suite are obtained using pressures between 2–4 kbar, which correspond to crustal depths of roughly 7–15 km, assuming a crustal density of 2800 kg/m^3 and only lithostatic pressure. Varying the pressure mainly affects the stability of plagioclase and clinopyroxene, with lower pressure favoring plagioclase. The initial temperature of the parental melt was the liquidus temperature as defined by the MCS in the beginning of each run. For the wall rock initial temperature, we assumed a linear pre-intrusion geotherm of 27 °C/km, which is close to a typical

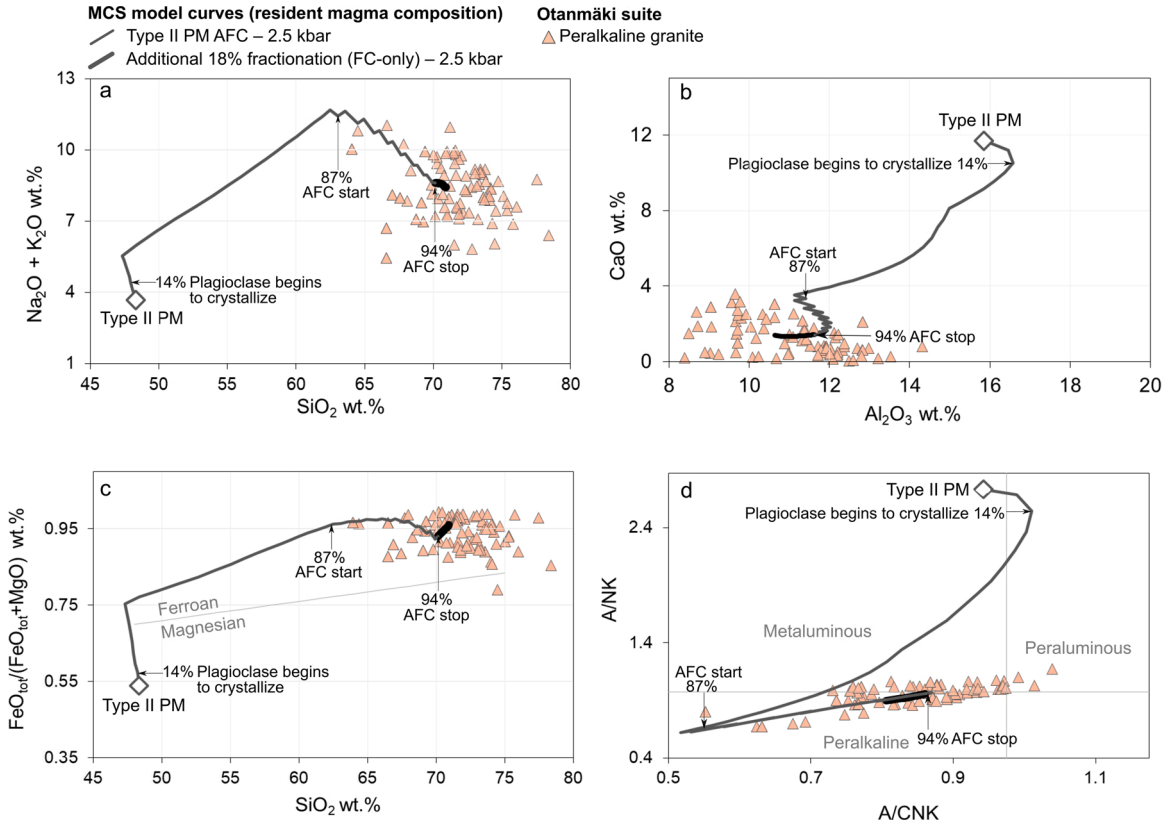

Fig. 13. Major element evolution of resident magma in Magma Chamber Simulator (MCS) assimilation fractional crystallization (AFC) model using the type II parental magma (PM) composition and tonalite wall rock compared to Otanmäki suite peralkaline granite in a) total alkali vs. SiO_2, b) CaO vs. Al_2O_3, c) FeO_{tot}/(FeO_{tot}+MgO) vs. SiO_2, and d) A/NK vs. A/CNK diagrams. Also shown is the resident magma composition produced by additional fractionation of the final melt generated by the AFC model. The degree of crystallization relative to the mass of the parental melt in selected crystallization steps, initiation of plagioclase crystallization and points where assimilation begins and stops is also indicated.

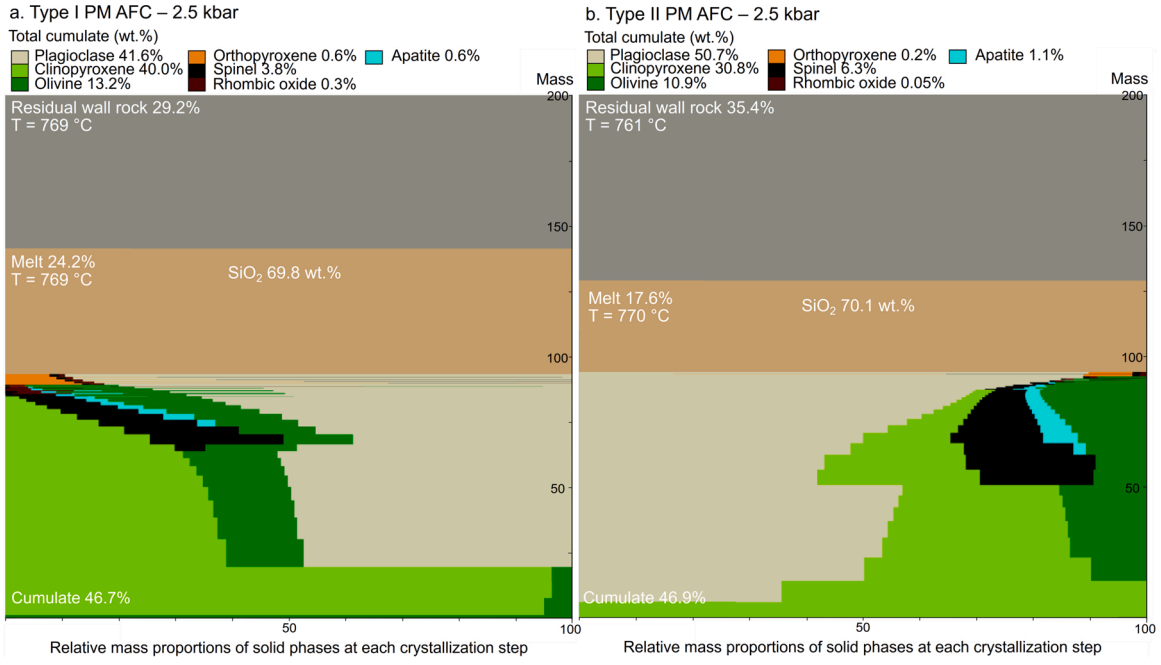

Fig. 14. Cumulate sequences at the end of representative Magma Chamber Simulator (MCS) assimilation fractional crystallization (AFC) models using the type I (a) and type II (b) parental magma (PM) compositions and tonalite wall rock. Model evolution is bottom-up (i.e., earliest cumulates at the bottom, final residual melt at the top). Note that the percentages and the relative proportions reflect mass and not area or volume. The SiO_2 content and temperature of the residual melt are also indicated. Figures were created using the MCS Visualizer Tool available from the MCS website (https://mcs.geol.ucsb.edu/).

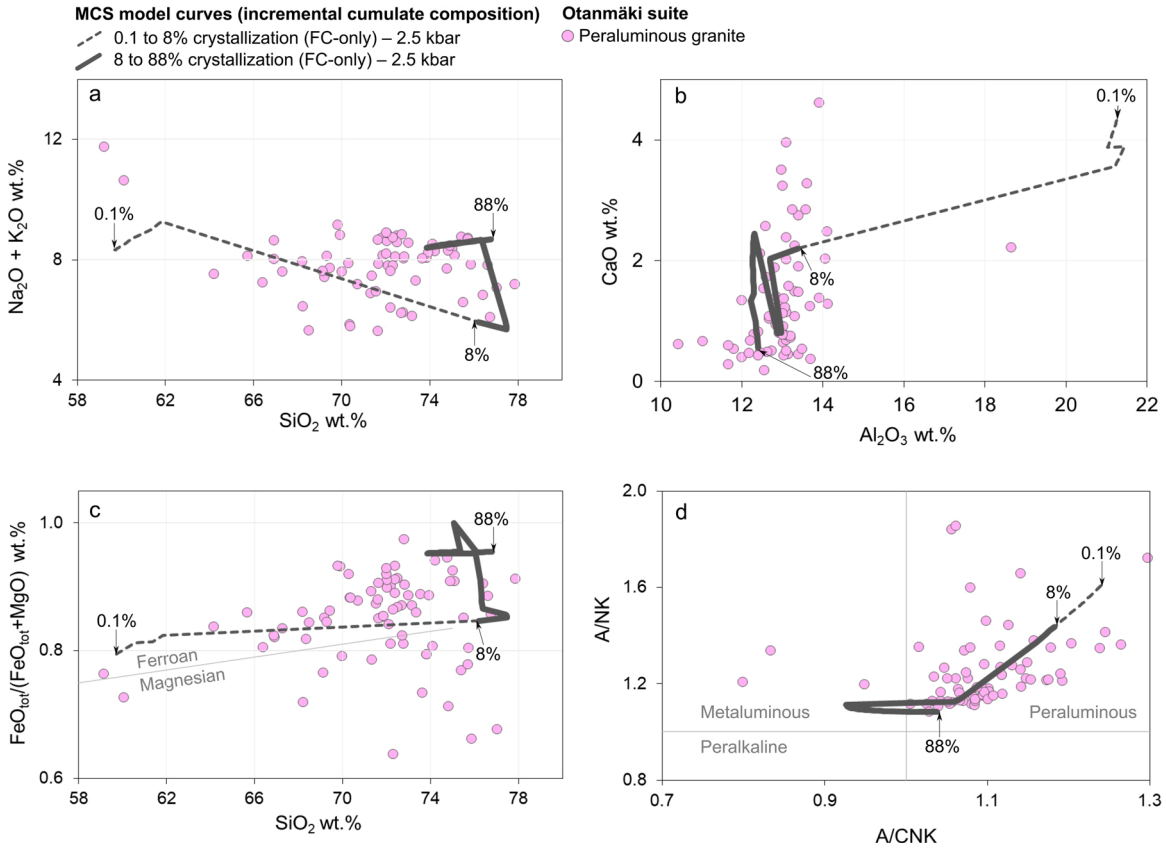

Fig. 15. Major element evolution of incremental cumulates in Magma Chamber Simulator (MCS) assimilation fractional crystallization (AFC) model using peraluminous high-silica melt composition (the final product of the "Type I PM AFC – 2.5 kbar" model, see Fig. 12; Table 5) compared to Otanmäki suite peraluminous granite in a) total alkali vs. SiO_2, b) CaO vs. Al_2O_3, c) $FeO_{tot}/(FeO_{tot}+MgO)$ vs. SiO_2, and d) A/NK vs. A/CNK diagrams. The degree of crystallization relative to the mass of the starting melt in selected crystallization steps is also indicated.

geothermal gradient within the upper continental crust, corresponding to 200 °C at 2 kbar (~7 km) and 400 °C at 4 kbar (~15 km). Lowering the initial wall rock temperature allows longer periods of FC-only evolution before the magma is heating up the wall rock above its solidus and coupled assimilation and fractional crystallization begins. For the melt percolation threshold, we used a value of 8% given in the default input file in all runs, as the test runs showed that varying the threshold value had only a negligible effect on the modeling outcomes, unless very high values were used (>50%). For modeling purposes, the mass of the parental melt and wall rock was 100 units (g) in all runs (Table 5). In the case of AFC and assuming a hypothetical spherical magma body with a diameter of 2 km, this means a wall rock zone with a total thickness of ~250 m available for magma-wall rock interaction. Magma recharge was precluded from the models, as new pulses of hot, more primitive magma added to the resident magma would effectively counteract the effects of fractionation and assimilation, inhibiting the production of highly evolved magmas, which is required in modeling of the Otanmäki suite.

6.5. Modeling results

Results of the FC and AFC modeling using MCS are illustrated in Figs. 9–17 and Table 5, and all the input and output data are presented in Electronic Appendix C. In the following discussion, we concentrate on the major oxides SiO_2, Al_2O_3, FeO_{tot}, MgO, CaO, Na_2O, and K_2O, which appear relatively little affected by secondary alteration (Kärenlampi et al., 2019). Subsequent trace element (Nb, Nd, U) and Nd isotope modeling was only performed for the best-fit major element models.

6.5.1. Fractional crystallization modeling

Our FC runs show that the modeled crystallization paths are generally similar for both the type I and type II parental melts, especially in the early stage. The first stage in the crystallization sequence (~1200–1050 °C) involves an extensive removal of clinopyroxene, olivine and plagioclase until ~60–70% of the mass of the parental melt has crystallized, producing a strong depletion in MgO and CaO and an increase in FeO_{tot}, SiO_2, Al_2O_3, Na_2O, K_2O and Fe-index in the resident magma (Figs. 9a–b, 10 a–d). This induces stabilization of calcic plagioclase and minor amounts of olivine, Ti-rich spinel (i.e., titanomagnetite), apatite, and alkali feldspar, whereas the crystallization of clinopyroxene is suppressed. The late plagioclase fractionation results in a depletion in Al_2O_3 and CaO and an increase in SiO_2, Na_2O and K_2O in the resident magma, which becomes increasingly more peralkaline as the A/NK and A/CNK ratios in the magma decrease (Fig. 10). This is known as the "plagioclase effect" (Bowen, 1945). The FC-only runs also demonstrate that the variation in the parental melt composition has a significant effect on the major element evolution and phase equilibria. The models run with the type I parental melt yield higher initial MgO and CaO contents (Table 4) increasing the stability of clinopyroxene and olivine relative to that of plagioclase and spinel, whereas in the type II parental melt runs, the situation is the opposite (Figs. 9a–b). Because of this, the plagioclase effect is stronger in the case of type II parental melt.

It is evident from our FC models that the modeled melt compositions having the best-fit with the major element compositions of the Otanmäki suite intermediate rocks were produced by a high degree of fractionation of the type I parental melt in the 3–4 kbar range, with the 3.5 kbar run providing the closest match (Figs. 9a,10, Table 5), whereas the models using type II parental melt resulted in too low Al_2O_3. The syenite composition requires 92% fractionation of the parental melt whereas the

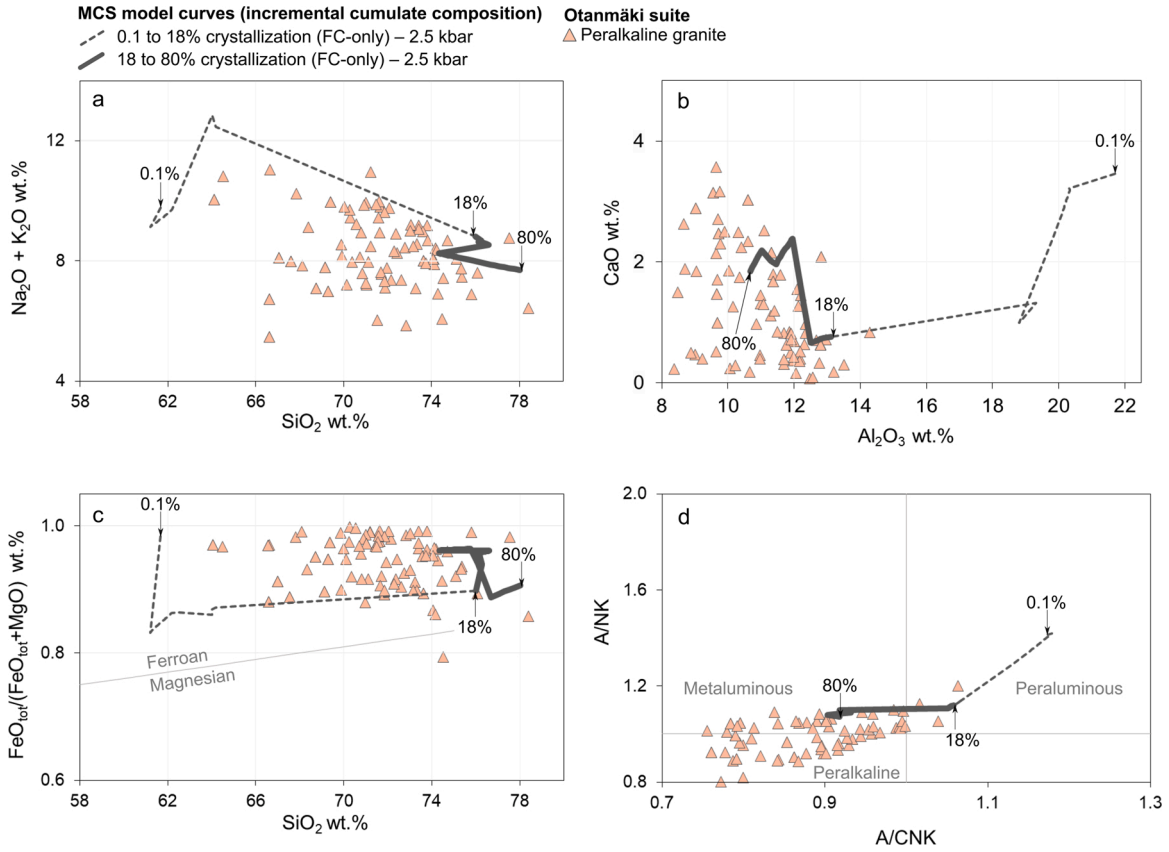

Fig. 16. Major element evolution of incremental cumulates in Magma Chamber Simulator (MCS) assimilation fractional crystallization (AFC) model using peraluminous high-silica melt composition (the final product of the "Type II PM AFC – 2.5 kbar" model, see Fig. 13; Table 5) compared to Otanmäki suite peralkaline granite in a) total alkali vs. SiO_2, b) CaO vs. Al_2O_3, c) $FeO_{tot}/(FeO_{tot}+MgO)$ vs. SiO_2, and d) A/NK vs. A/CNK diagrams. The degree of crystallization relative to the mass of the starting melt in selected crystallization steps is also indicated.

monzodiorite and monzonite compositions are formed by 74–85% fractionation, respectively (Fig. 10; Table 5). It should also be noted that it is possible that the intermediate rocks represent some kind of cumulate rocks from the type I parental melt. The compositions of the incremental cumulates of the best-fit FC model run are presented in Fig. 11. The modeled late cumulates are compositionally similar to the intermediate rocks implying that they may well represent various mixtures of cumulus minerals (Fig. 11) and residual melts (Fig. 10). This would be compatible with their relatively low incompatible trace element contents, which are similar or lower than in the OIB-like mafic dikes and the used parental melt compositions (Figs. 5a–b, e). Because this uncertainty in their absolute concentrations, trace elements were not modeled in detail here. Nevertheless, the depletions in Sr, P, and Ti in the trace element pattern of the syenite samples (Fig. 5b) are consistent with prior fractionation of plagioclase, apatite, and oxides as implied by the MCS models. The characteristic Ba enrichment, especially in the monzodioritic-monzonitic rocks (Fig. 5a), cannot be easily explained by fractionation and likely requires heterogeneity in the

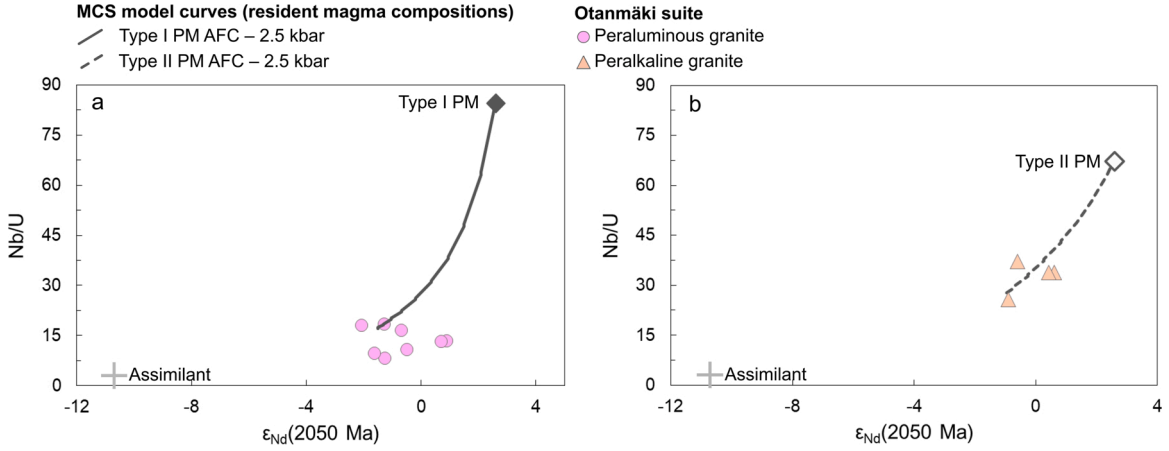

Fig. 17. Nb/U and ε_{Nd}(2050 Ma) data of Otanmäki suite granite samples compared with resident magma compositions generated in Magma Chamber Simulator (MCS) assimilation fractional crystallization (AFC) models (see Figs. 13 and 14) using type I and type II parental magma (PM) and tonalite assimilant compositions.

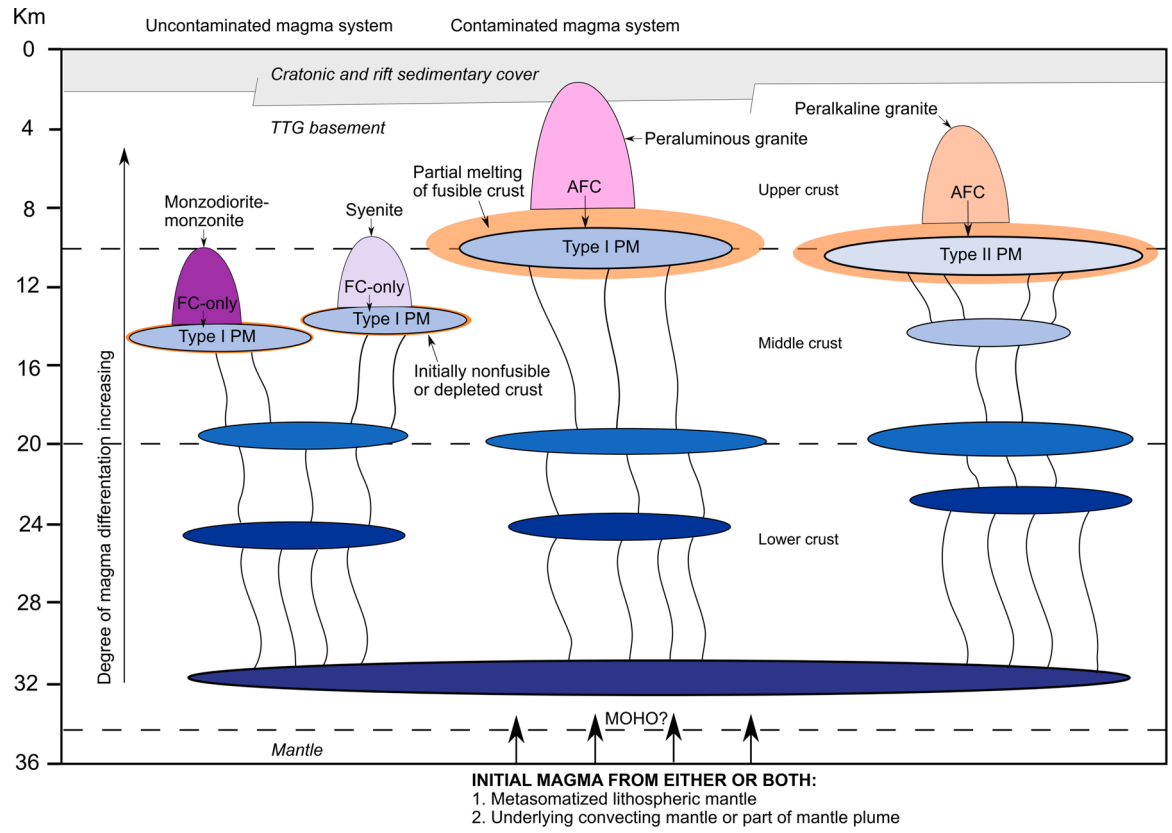

Fig. 18. A schematic model of the petrogenesis of Otanmäki suite A1-type granites and associated intermediate rocks (monzodiorite-monzonite, syenite) by differentiation of mantle-derived parental magmas in the middle to upper crust (~2–4 kbar, ~7–15 km). The intermediate rocks were formed by fractional crystallization (FC) of type I parental magma (PM) involving crystallization of large amounts of clinopyroxene, plagioclase and olivine with minimal crustal contamination. The generation of the granites requires further fractional crystallization of their parental magmas coupled with assimilation of partial melts from fusible quartzofeldspathic crust, such as Archean tonalite. The peraluminous granite was generated by assimilation fractional crystallization (AFC) from a relatively primitive parental magma (type I), which produced more clinopyroxene and olivine relative to plagioclase alongside with assimilation of high-silica partial melts from Archean tonalite. In contrast, the genesis of the peralkaline granite requires a high degree of AFC of an already fractionated parental magma (type II), involving crystallization of a plagioclase-dominated mineral assemblage in the subsequent fractionation processes.

mantle source. Such heterogeneity in fluid-mobile elements has been suggested for subcontinental mantle sources elsewhere (e.g., Rogers et al., 1987; Ersoy et al., 2010; Wang et al., 2016; Heinonen et al., 2018), but some effects of secondary alteration cannot be completely ruled out either.

6.5.2. *Assimilation fractional crystallization (AFC) modeling*

On the basis of the observed trace element signatures, Nd isotope compositions, SiO_2 enrichment and variation in alkalinity/aluminosity in the granitic rocks in the Otanmäki suite, assimilation of Archean wall rocks had a pivotal role in their petrogenesis. As the granite bodies in the Otanmäki suite appear to be devoid of xenoliths or restites, it is most likely that the assimilation took place by mixing with partial melts from the wall rocks instead of bulk assimilation.

Results of the MCS modeling involving assimilation are illustrated in Figs. 12–17. Compared to the FC-only models at the same pressure, the AFC models generate magmas with higher SiO_2, lower or similar Al_2O_3 and CaO and lower Na_2O and K_2O (Figs. 12 and 13). This is because the main contributing phases to the wall rock partial melts are quartz, sodic plagioclase, potassium feldspar, and biotite. The model-generated wall rock melts are high in SiO_2, peraluminous and ferroan to slightly magnesian, although they are very low in mafic components (Table 4). It is important to note that the wall rock partial melt compositions generated in our MCS-based AFC models are similar to the melts reported to be produced in experimental dehydration melting of tonalite (Patiño Douce, 1997). At the same pressures, the parental melt crystallization behavior is essentially the same in both the FC-only and AFC models, i.e., more plagioclase relative to clinopyroxene and olivine is produced from the type II parental melt relative to type I parental melt (Figs. 9 and 14). However, in the AFC models, the addition of wall rock melts causes a greater enrichment in SiO_2 and more effective increase in the A/NK and A/CNK ratios of the resident melt. The AFC models demonstrate that melt compositions most similar to the Otanmäki suite granites require a high degree of fractionation of the parental melts (93–95%) in the 2.0–2.5 kbar pressure range, with the 2.5 kbar runs providing the closest match (Figs. 12–13, Table 5). The magma compositions generated using the type II parental melt correspond most closely to the Otanmäki suite peralkaline granite. This is mainly because the type II parental melt composition enabling high amount of plagioclase fractionation (Fig. 14) that functions against the increase in A/NK and A/CNK in the magma caused by the addition of wall rock liquids (Fig. 13). In contrast, peraluminous silicic model melts similar to those of the Otanmäki suite are favorably produced from the type I parental melt AFC models, in which the late plagioclase removal delays this effect (Figs. 12 and 14). Our AFC models suggest that just by varying the parental melt composition, while keeping the amount and composition of the assimilated crustal material relatively similar (Table 5), the model melt trends approach both the peralkaline and peraluminous granitic compositions (Figs. 12–13), suggesting that their derivation by AFC processes from a mafic magma is plausible. However, the models fail to

Table 5
Mass constraints of parental magma (PM), cumulate, and wall rock (WR) subsystems in the FC-AFC models and model generated remaining magma major element compositions.

Model	Mass constraints (g)						Remaining magma major element composition (wt.%)									Remaining magma TE (ppm) and Nd isotopic composition				
	Parental magma	Remaining magma	Cumulates	Wall rock	Wall rock partial melt added to magma	R	SiO_2	Al_2O_3	FeO_{tot}	MgO	CaO	Na_2O	K_2O	A/NK	A/CNK	Fe*	Nb	U	Nd	$^{143}Nd/^{144}Nd$ (2050 Ma)	ε_{Nd} (2050 Ma)
FC runs																					
Monzodiorite																					
Type I PM - 3.0 kbar	100	26	74	–	–	–	49.4	17.4	11.5	3.1	7.5	3.9	2.3	1.95	1.11	0.79	–	–	–	–	–
Type I PM - 3.5 kbar	100	26	74	–	–	–	48.8	17.8	11.5	3.1	7.5	3.9	2.3	1.99	1.13	0.79	–	–	–	–	–
Type I PM - 4.0 kbar	100	24	76	–	–	–	49.0	18.5	11.1	2.9	7.0	4.1	2.5	1.96	1.17	0.80	–	–	–	–	–
Monzonite																					
Type I PM - 3.0 kbar	100	16	84	–	–	–	55.3	16.7	8.6	1.3	5.4	4.7	3.7	1.42	1.00	0.87	–	–	–	–	–
Type I PM - 3.5 kbar	100	15	85	–	–	–	55.5	17.0	8.1	1.1	4.9	4.8	4.0	1.39	1.02	0.88	–	–	–	–	–
Type I PM - 4.0 kbar	100	13	87	–	–	–	55.5	17.6	7.8	0.9	4.3	5.1	4.4	1.34	1.03	0.90	–	–	–	–	–
Syenite																					
Type I PM - 3.0 kbar	100	9	91	–	–	–	61.6	14.6	4.8	0.2	3.4	5.2	6.0	0.97	0.81	0.96	–	–	–	–	–
Type I PM - 3.5 kbar	100	8	92	–	–	–	61.4	15.0	4.3	0.1	2.9	5.1	6.5	0.97	0.83	0.98	–	–	–	–	–
Type I PM - 4.0 kbar	100	5	95	–	–	–	59.6	14.8	4.1	0.01	2.7	6.3	5.7	0.89	0.78	1.0	–	–	–	–	–
AFC runs																					
Peraluminous granite																					
Type I PM - 2.0 kbar	100	32	93	100	25	0.3	70.1	12.8	1.2	0.1	1.6	3.3	4.9	1.20	1.06	0.90	–	–	–	–	–
Type I PM - 2.5 kbar	100	48	93	100	42	0.4	69.8	12.9	1.2	0.2	1.5	3.8	4.0	1.22	1.08	0.88	76	3.5	80	0.509894	−1.8
Peralkaline granite																					
Type II PM - 2.0 kbar	100	23	95	100	19	0.2	71.2	10.6	1.4	0.1	1.6	4.5	4.5	0.87	0.78	0.93	–	–	–	–	–
Type II PM - 2.5 kbar	100	35	94	100	29	0.3	70.1	11.6	1.5	0.1	1.4	4.5	4.1	0.98	0.89	0.93	190	5.9	108	0.509919	−1.3

R = ratio of cumulates to assimilated rock, A/NK = molar $Al_2O_3/(Na_2O + K_2O)$, molar A/CNK = $Al_2O_3/(CaO + Na_2O + K_2O)$, Fe* = $FeO_{tot}/(FeO_{tot} + MgO)$ wt.%, TE = trace element.

reach the highest SiO_2 contents in the magma series as in the current version of MCS, the AFC simulations halt when thermal equilibrium between the resident magma and wall rock is attained and therefore, terminal crystallization sequences of the contaminated residual melts cannot be obtained from the AFC models, but require additional FC-only modeling of the final residual melt (see below).

At the end of modeling, we made additional FC-only runs starting from the final peraluminous and peralkaline high-silica melt (~70 wt.% SiO_2) compositions produced in the 2.5 kbar AFC runs (Table 5). The runs achieved near complete crystallization of the melts (~80–88%). The first stage of fractionation (~10–20%) is dominated by calcic plagioclase and minor Fe-Ti-rich spinel, rhombic Fe-Ti oxide, and orthopyroxene, which causes a slight increase in SiO_2 and a slight decrease in Al_2O_3, CaO, FeO_{tot}, and Na_2O but without a significant change in A/NK and A/CNK of the residual melts, resulting in melt compositions even more akin to the Otanmäki suite granites (Figs. 15–16). This change in the melt compositions induces stabilization of alkali-rich feldspars and quartz along with minor Fe-rich minerals (e.g., fayalite, pyroxenes, Fe-Ti-rich spinel and rhombic oxide), which dominate the latter part of crystallization. From this point onwards, the incremental cumulate compositions produced from both the peralkaline and peraluminous starting melt compositions are ferroan, very high in silica (~74–78 wt.% SiO_2), and peraluminous to slightly metaluminous but not peralkaline (Figs. 15–16). This indicates that crystal accumulation would increase the SiO_2 content and aluminosity of the granite magmas, and that peraluminous granite compositions, unlike peralkaline, could to some extent represent various mixtures of cumulus minerals and residual melts.

Like in the case of the FC-only models, the uncertainties regarding the possible cumulate nature of the granitic rocks hamper the modeling of their trace element evolution. Nevertheless, since incompatible trace element ratios, such as Nb/U, and Nd isotope compositions are not affected by fractionation or accumulation of major phases recognized in the models, but are highly influenced by assimilation processes, they provide a more straightforward avenue. We modeled their behavior in the AFC simulations. Input (including partition coefficients) and output data are given in Tables 2,4 and 5 and Electronic Appendix C and the modeling results are illustrated in the Nb/U vs. ε_{Nd}(2050 Ma) diagrams shown in Fig. 17. As seen in Fig. 17, the best-fit models using type I and II parental melt compositions and Archean tonalitic wall rock produce the Nb-U systematics and Nd isotopic compositions of the peralkaline granites relatively well, demonstrating their origin by AFC of an OIB-like mafic magma viable. In the case of the peraluminous granites, the standard model fails to reach the lowest Nb/U ratios shown by them. This could be explained by 1) a parental melt formed by higher-degree of mantle melting (and thus having lower initial incompatible element concentrations) than the one used in the model, 2) assimilant more enriched in incompatible trace elements than the one used in the model, or 3) the effect of possible HFSE-bearing accessory minerals not recognized by MELTS in the melting wall rock.

7. Discussion

7.1. Petrogenetic implications

The presented geochemical and Nd isotopic data and numerical modeling provide a good foundation on deciphering the sources and petrogenetic pathways of the Otanmäki suite of A1-type granitic and intermediate igneous rocks emplaced in the same igneous complex. Based on the MCS modeling, extensive fractional crystallization of mantle-derived magmas with minimal crustal contamination can plausibly generate the intermediate rocks. Instead, the generation of the granites requires fractional crystallization combined with assimilation, which likely took place in the middle to upper crust (~2–4 kbar, ~7–15 km; Fig. 18), where Archean wall rocks were available and mafic parental magmas were able to crystallize extensive amounts of clinopyroxene, plagioclase and olivine. A relatively cool geotherm may have been a contributing factor enabling extensive fractionation before the wall rocks were heated above their solidus. Furthermore, the wide spectrum of daughter melt compositions present in the Otanmäki A1-type suite opposes the view that the magma chambers supplying magma to the A1-type plutons were continuously replenished and tapped, as these processes would effectively inhibit the generation of highly fractionated magmas and instead result in steady-state (mafic) compositions (cf. Mourtada-Bonnefoi et al., 1999; Petrone et al., 2018). Therefore, the formation of the A1-type magmas was likely related to rapidly filled and relatively large magma chambers, in which the magma evolved essentially through crystal-melt fractionation with varying crustal interaction.

The chemical composition of the parental melts is also an important variable. In our models, we used the OIB-like alkaline mafic dikes from the Otanmäki area to construct the parental melt starting compositions because, from many tentatively tested candidates, they provided evolved daughter compositions most similar to the Otanmäki suite granites and intermediate rocks. Several trace element diagrams (Figs. 5–7) demonstrate that the A1-type rocks and the OIB-like mafic dikes form a continuum of compositions, which is a strong indication of a genetic relationship. Also, the fact that these mafic dikes occur in the study area supports the idea that these dikes provide a strong clue of what could have been the parental magmas to the A1-type rocks. The FC-AFC runs also show that the initial compositions of the parental magma prior to the extensive differentiation and assimilation in the middle to upper crust has a significant effect on the differentiation paths and final products of the differentiation process. The compositions of the alkaline OIB-type mafic dikes used as proxies to the parental magma composition show a considerable variation in their Mg-numbers (Tables 3 and 4), suggesting that the parental melts probably evolved at greater depths, possibly in the lower crust or mantle-crust boundary, already prior to their emplacement at a shallower crustal level. This implies that the precursor parental magmas themselves were products of fractionation of a more primitive parent. Thus, a significant mafic magma reservoir could have been situated at depth, supplying batches of magma that evolved towards intermediate to felsic compositions in shallow crustal magma reservoirs or traveled directly towards the surface to form dikes, or alternatively, the degree of melting in the mantle source for the magmas in different dikes was variable. A similar situation has been suggested for many other magmatic systems, such as in oceanic eruptive centers with mafic and intermediate to felsic magmatism (e.g., Chen et al., 2013; Jeffery and Gertisser, 2018 and references therein).

The above discussed findings can be applied to explaining the origin of the variation in the alkalinity and aluminosity of the Otanmäki suite granites. The peraluminous granite was generated by AFC from a relatively primitive parental magma, which produced more clinopyroxene and olivine relative to plagioclase alongside with assimilation of high-silica partial melts from Archean tonalite. In contrast, the genesis of the peralkaline granite requires a high degree of AFC of an already fractionated parental magma, involving crystallization of a plagioclase-dominated mineral assemblage in the subsequent fractionation processes. This interpretation is supported by the observation that the Zr/Ti ratios and concentrations of incompatible elements (e.g., Zr, Nb, REE) are highest in the peralkaline granite relative to the other A1-type rocks in the Otanmäki suite, which likely denotes significantly higher degree of differentiation in its parental magma. The trace element modeling of the peraluminous high-silica magmas pointed out that it is likely that their parental magmas were less enriched in U-Nb than those used in the models, either being derived from a different source or via a higher degree of melting of the same source as the OIB-like mafic dikes used as a proxy. Even a small change in the degree of melting in the mantle source can produce significantly different highly incompatible trace element concentrations in the generated melt but without noticeable change in the major element concentrations (e.g., Heinonen et al., 2016; Spandler et al., 2017). Usually low-degree mantle-derived melts in continental

settings show less trace element and isotopic evidence for crustal contamination than more voluminous high-degree melts that possess more thermal energy and are more likely to pool in large crustal magma chambers and evolve by FC and AFC (e.g., Krienitz et al., 2007). It is also relevant to discuss what may have been the controlling factors in the generation of the granites through AFC and why the intermediate rocks record relatively little assimilation. It is not uncommon to find both contaminated and uncontaminated igneous rocks in the same province because of multiple reasons (e.g., Meshesha and Shinjo, 2007; Shellnut, 2014; Luttinen, 2018). In the Otanmäki case, the simplest explanation could be that the parental magmas of the intermediate rocks encountered wall rocks that were either initially nonfusible or had their melt-production capacity lowered by early heating events (cf. Meade et al., 2014), possibly related to the petrogenesis of the associated granites. Alternatively, the parental melts may have remained relatively uncontaminated if they migrated through feeder channels armored by early magmatic events (cf. Riishuus et al., 2008).

Regarding analogous A1-type systems globally, the Red Sea A1-type granite is one of the most interesting example, as it shows chemical variation similar to that in the Otanmäki suite (see Kärenlampi et al., 2019). The genesis of these plutons with A1-type peralkaline to peraluminous granite and syenite compositions have also been interpreted in terms of AFC processes involving an OIB-type alkali basaltic parental magma and assimilation of Proterozoic continental crust, which consists mostly of amphibolite-facies orthogneisses and supracrustal rocks (Coleman et al., 1992; Tommasini et al., 1994; Chazot and Bertrand, 1995; Whitehouse et al., 2001). In the studies on the Red Sea granite, AFC processes have been examined using only isotopic and trace element data, which can be problematic as outcomes of such models rely largely on poorly-known partition coefficients without considering the related magma and wall rock phase equilibria. Nevertheless, comparison of the ratio of the assimilated and crystallized masses in our best-fit AFC models (0.3–0.4; Table 5) to that obtained iteratively in modeling the genesis of the magmas of the Red Sea granite (0.2–0.3; Tommasini et al., 1994) reveals that they are in good agreement, although in the Red Sea models, there is some uncertainty because of the large number of potential assimilant compositions (Tommasini et al., 1994; Chazot and Bertrand, 1995).

The results of our AFC modeling support the general perception that A-type granitic magmas become peraluminous by involvement of partial melts of quartzo-feldspathic crust, such as TTG basement (e.g., Frost and Frost, 2011), but not necessarily the proposition made in some previous studies that peraluminous granites would record more crustal assimilation than metaluminous or peralkaline variants in the same igneous complex (Frost and Frost, 2011; Dall'Agnol et al., 2012 and references therein). However, other thermodynamically constrained modeling studies of the genesis of A-type granites (e.g., Shellnutt et al., 2011; Shellnutt and Dostal, 2020) have succeeded in modeling generation of peralkaline and peraluminous A-type granite compositions by direct fractional crystallization of OIB-type and subalkaline mafic parental magma starting compositions, respectively, without involving crustal contamination. Therefore, it is still possible that in the Otanmäki case, the parental melt of peraluminous granite was petrogenetically unrelated or distant to that of the peralkaline granite. Nevertheless, our thermodynamically constrained AFC modeling shows that both of them can be plausibly produced from OIB-like mafic parental melts if a similar difference in the parental melt compositions is allowed as is recorded by the compositional variation of the spatially associated OIB-like mafic dikes, and assuming similar amounts of crustal contamination.

7.2. Mass and volume perspectives

The constructed FC-AFC models enable us to approximate the relative volumes of each of the main subsystems involved in the genesis of the Otanmäki suite magma series (magma, cumulates, wall rock liquid and solids) and then to compare them with the estimated volumes of each igneous phase present in the suite. Although the occurrence of Otanmäki suite A1-type rocks in fault-bounded and fault-pierced, possibly rootless tectonic bodies considerably hampers such an evaluation, it would nevertheless give a rough idea of that how well the model-predicted original magma system is preserved in the present suite.

According to the mapped surface areas (Fig. 2b; for calculation see Electronic Appendix D), the peraluminous granite (148 km^2, 65%) dominates the suite, with the peralkaline granite being the second most common (60 km^2, 26%) and the intermediate rocks only forming a minor component (17 km^2 8% syenite, 1.2 km^2, 1% monzodiorite-monzonite). A calculation assuming these areas for the rock types and conservatively an average minimum depth extent of 0.5 km for the whole system, yields the following hypothetical volumes: 74 km^3 peraluminous granite, 30 km^3 peralkaline granite, 8.6 km^3 syenite, and 0.6 km^3 monzodiorite-monzonite. It must be said that these estimates are only tentative due to checkered exposure and poorly known depth continuations of the rock units. However, as the average thickness of the main nappe was before the obvious erosion losses likely more than the 0.5 km applied above, the above calculated volumes could be considered rather minimum than maximum estimates of the volumes that were present in the original magma system. In comparison, a single-stage FC model applied to an intrusive volume of 100 km^3 of mafic parental magma could generate at least ~30 to 15 km^3 of monzodiorite or monzonite (respectively) or ~10 km^3 of syenite, whereas a AFC model could generate ~55 km^3 of peraluminous granite or ~40 km^3 of peralkaline granite (for calculation see Electronic Appendix D). The volumes of the minerals predicted to crystallize as dominantly mafic cumulates prior to the generation of intermediate to felsic derivate magmas can be calculated using an iteratively selected multiplier that, within the mass constraints of the FC-AFC models, produces the above-estimated volumes of the Otanmäki suite A1-type rocks. This calculation indicates that the predicted total volume of the complementary cumulates would be at least in the range ~200 km^3. However, the geophysical maps and deep seismic reflection survey data of the study area (e.g., Elo, 1997; Kozlovskaya and Yliniemi, 1999; Korja et al., 2006; Kontinen and Paavola, 2006) lack indications of such large volumes of dense mafic cumulates (ρ = ~3.02–3.16 g/cm^3), which is in marked contrast to the situation with many other A-type igneous complexes that tend to either occur with significant masses of coeval/cogenetic mafic rocks (e.g., Coleman et al., 1992; Shellnutt et al., 2011) or at least exhibit prominent positive gravity anomalies indicating such in the depth (e.g., Smith et al., 1999; Anderson et al., 2003). There are several possible explanations to the puzzling lack of mafic rocks in the Otanmäki case: 1) The A1-type rocks were not produced by FC and/or AFC of mantle-derived magmas, which we consider unlikely based on our modeling; 2) The cumulates are present but located sufficiently deep in the crust or within other mafic rock types so that they are not observable by the present geophysical data; 3) The main nappe and lens-shaped body containing the A1-type rocks represent exotic rootless allochthons thrust without the mafic cumulates from the west of the Svecofennia-Karelia boundary. This latter option is supported by the fact that 2.05 Ga felsic A1-type rocks similar to those of the Otanmäki suite are unknown from the surrounding bedrock units. Even potential candidates for such rocks are very scare, limited to few narrow and undated granitic dikes in the Otanmäki gabbro.

8. Conclusions

1) The ca. 2.05 Ga peralkaline to peraluminous granites and associated intermediate igneous rocks (monzodiorite -monzonite, syenite) of the Otanmäki suite exhibit geochemical characteristics consistent with derivation by differentiation of mantle-derived OIB-type magmas with a variable degree of interaction with crustal material. The intermediate rocks show positive initial ε_{Nd} (2050 Ma) values (+1.3 to +2.6), which are only slightly lower than the estimated value for the contemporaneous depleted mantle but much higher

than ε_{Nd}(2050 Ma) of Archean TTGs in the surrounding bedrock, demonstrating that these rocks were derived from a mantle source without notable crustal involvement. The ε_{Nd}(2050 Ma) values of the peralkaline and peraluminous granite samples show a considerable overlap (–0.9 to +0.6 and –3.2 to +0.9, respectively) and are somewhat lower than those of the intermediate rocks, suggesting that their mafic parental magmas assimilated some older Archean continental crust during their fractionation.

2) Numerical modeling with the Magma Chamber Simulator shows that fractional crystallization (FC) of mantle-derived magmas can explain the geochemical characteristics of intermediate igneous rocks but alone cannot explain the key characteristics of the granites. The genesis of the latter requires an assimilation-fractional crystallization (AFC) process involving contamination with Archean crustal material, which must have taken place in the middle to upper crust (~2–4 kbar, ~7–15 km), where suitable Archean wall rocks were available and mafic parental melts were able to crystallize extensive amounts of clinopyroxene, plagioclase and olivine. The models generated in this study predict the presence of complementary cumulates with a volume doubling that of related intermediate and granitic rocks. Since such rocks are not known to exist in the area or at depth, the idea of the Otanmäki suite being part of a rootless allochthon is supported.
3) The outcomes of our FC-AFC modeling are consistent with previous studies suggesting that magmas of A-type ferroan granites become more peraluminous by involvement of partial melts of quartzofeldspathic crust, such as Archean tonalite. However, we found that in addition to differing amounts of assimilated crustal melts, the variations in alkalinity and aluminosity in the end product high-silica magmas can also depend on the quantity of late plagioclase fractionation. Peralkaline high-silica magmas are a manifestation of a strong plagioclase effect in the mafic parental melt, buffering the increase in A/NK and A/CNK caused by the assimilated crustal melts. By contrast, peraluminous high-silica compositions are derived by AFC from a mafic parental melt which only produces a moderate/weak plagioclase effect, resulting in relatively low-alkalinity residual magmas with high A/NK and A/CNK ratios.

Credit author statement

The contributions of the first author and the co-authors in the manuscript

The main responsibility for the conceptualization, methodology, manuscript preparation and interpretation was carried by Kimmo Kärenlampi with other authors contributing. Kimmo Kärenlampi was responsible of the Magma Chamber Simulator thermodynamic modeling and interpretation with Jussi S. Heinonen contributing to the modeling and interpretation of modeling results. Asko Kontinen and Eero Hanski contributed in supervision and preparation and reviewing the manuscript. Hannu Huhma was responsible for the Sm-Nd analysis conducted at the GTK and Finnish Isotope Geoscience laboratory and contributed to the interpretation of Sm-Nd data.

Declaration of Competing Interest

The authors declare that they have no known competing financial interests or personal relationships that could have appeared to influence the work reported in this paper.

Acknowledgements

Financial support to Kimmo Kärenlampi was provided by the Advanced Materials Doctoral Programme (ADMA-DP) of the University of Oulu, K.H. Renlund Foundation and Tauno Tönning Foundation, and Jussi S. Heinonen by the Academy of Finland (Grant no. 295129). The field work was supported by Otanmäki Mine Oy (www.otanmaki.fi) and Jouko Jylänki, the CEO of the company, which is gratefully acknowledged. Yann Lahaye, Leena Järvinen, and Hugh O'Brien from the GTK are thanked for laboratory assistance. Gregory Shellnutt, Bernard Bonin, and two anonymous reviewers and the handling editor Astrid Holzheid are thanked for their constructive comments that helped to improve this manuscript.

Appendices A–D. Supplementary data

Supplementary material related to this article can be found, in the online version, at doi:https://doi.org/10.1016/j.chemer.2020.125734.

References

Ahtonen, N., Hölttä, P., Huhma, H., 2007. Intracratonic Palaeoproterozoic granitoids in northern Finland: prolonged and episodic crustal melting events revealed by Nd isotopes and U-Pb ages on zircon. Bull. Geol. Soc. Finl. 79, 143–174. https://doi.org/10.17741/bgsf/79.2.002.

Anderson, I.C., Frost, C.D., Frost, B.R., 2003. Petrogenesis of the red mountain pluton, laramie anorthosite complex, Wyoming: implications for the origin of A-type granite. Precambrian Res. 124, 243–267. https://doi.org/10.1016/S0301-9268(03)00088-3.

Bacon, C.R., Druitt, T.H., 1988. Compositional evolution of the zoned calcalkaline magma chamber of Mount Mazama, crater Lake. Oregon. Contrib. Mineral. Petrol. 98, 224–256. https://doi.org/10.1007/BF00402114.

Bea, F., Pereira, M.D., Stroh, A., 1994. Mineral/leucosome trace-element partitioning in a peraluminous migmatite (a laser ablation-ICP-MS study). Chem. Geol. 117, 291–312. https://doi.org/10.1016/0009-2541(94)90133-3.

Beard, J.S., Ragland, P.C., Rushmer, T., 2003. Hydration crystallization reactions between anhydrous minerals and hydrous melt to yield amphibole and biotite in igneous rocks: description and implications. J. Geol. 112, 617–621. https://doi.org/10.1086/422670.

Bedrock of Finland – DigiKP, 2019. Digital Map Database (Electronic Resource). Espoo, Geological Survey of Finland. Version 2.2 13 September available at: https://gtkdata.gtk.fi/Kalliopera/index.html.

Boehnke, P., Watson, B.E., Trail, D., Harrison, M.T., Schmitt, A.K., 2013. Zircon saturation re-revisited. Chem. Geol. 351, 324–334. https://doi.org/10.1016/j.chemgeo.2013.05.028.

Bohrson, W.A., Spera, F.J., Ghiorso, M.S., Brown, G.A., Creamer, J.B., Mayfield, A., 2014. Thermodynamic model for energy-constrained open-system evolution of crustal magma bodies undergoing simultaneous recharge, assimilation and crystallization: the Magma Chamber Simulator. J. Petrol. 55, 1685–1717. https://doi.org/10.1093/petrology/egu036.

Bohrson, W.A., Spera, F.J., Heinonen, J.S., Brown, G.A., Scruggs, M.A., Adams, J.V., Takach, M.K., Zeff, G., Suikkanen, E., 2020. Diagnosing open-system magmatic processes using the Magma Chamber Simulator (MCS): part I—major elements and phase equilibria. Contrib. Mineral. Petrol. 175, 104. https://doi.org/10.1007/s00410-020-01722-z.

Bonechi, B., Perinelli, C., Gaeta, M., Tecchiato, V., Granati, S.F., 2017. Experimental constraints on amphibole stability in primitive alkaline and calc-alkaline magmas. Period. di Mineral. 86, 231–245. https://doi.org/10.2451/2017PM735.

Bonin, B., 2007. A-type granites and related rocks: evolution of a concept, problems and prospects. Lithos 97, 1–29. https://doi.org/10.1016/j.lithos.2006.12.007.

Boudreau, A.E., 1999. PELE – a version of the MELTS software program for the PC platform. Comp. Geosci. 25, 201–203. https://doi.org/10.1016/S0098-3004(98)00117-4.

Bowen, N.L., 1945. Phase equilibria bearing on the origin and differentiation of alkaline trends. Am. J. Sci. 243A 75–89.

Bucher, K., Frost, B.R., 2006. Fluid transfer in high-grade metamorphic terrains intruded by anorogenic granites: the Thor range. Antarctica. J. Petrol. 47, 567–593. https://doi.org/10.1093/petrology/egi086.

Chazot, G., Bertrand, H., 1995. Genesis of silicic magmas during tertiary continental rifting in Yemen. Lithos 36, 69–83. https://doi.org/10.1016/0024-4937(95)00012-5.

Chen, S.-S., Lee, S.-G., Lee, T.-J., Lee, Y.-S., Liu, J.-Q., 2013. Multi-stage magmatic plumbing system of the volcano: a case study from Ulleung Island, South Korea. Lithos 314–315, 201–215. https://doi.org/10.1016/j.lithos.2018.05.028.

Coleman, R.G., DeBari, S., Peterman, Z., 1992. A-type granite and the Red Sea opening. Tectonophysics 204, 27–40. https://doi.org/10.1016/0040-1951(92)90267-A.

Dall'Agnol, R., Frost, C.D., Rämö, T., 2012. IGCP Project 510 "A-type granites and related rocks through time": project vita, results, and contribution to granite research. Lithos 151, 1–16. https://doi.org/10.1016/j.lithos.2012.08.003.

Davidson, J., Turner, S., Plank, T., 2013. Dy/Dy*: variations arising from mantle sources and petrogenetic processes. J. Petrol. 54, 525–537. https://doi.org/10.1093/petrology/egs076.

DePaolo, D.J., 1981. Neodymium isotopes in the Colorado Front Range and crust-mantle evolution in the Proterozoic. Nature 291, 193–196. https://doi.org/10.1038/291193a0.

DePaolo, D.J., Wasserburg, G.J., 1976. Nd isotopic variations and petrogenetic models. Geophys. Res. Lett. 3, 249–252. https://doi.org/10.1029/GL003i005p00249.

Dixon, J.E., Clague, D.A., 2001. Volatiles in basaltic glasses from Loihi Seamount, Hawaii: evidence for a relatively dry plume component. J. Petrol. 42, 627–634. https://doi.org/10.1093/petrology/42.3.627.

Dixon, J.E., Leist, L., Langmuir, C., Schilling, J.G., 2002. Recycled dehydrated lithosphere observed in plume-influenced mid-ocean-ridge basalt. Nature 420, 385–389. https://doi.org/10.1038/nature01215.

Donskaya, T.V., Gladkochub, D.P., Sklyarov, E.V., Kotov, A.B., Larin, A.M., Starikova, A. E., Mazukabzov, A.M., Tolmacheva, E.V., Velikoslavinskii, S.D., 2018. Genesis of the paleoproterozoic rare-metal granites of the Katugin Massif. Petrol. 26, 52–71. https://doi.org/10.1134/S0869591118010022.

Dostal, J., 2016. Rare metal deposits associated with alkaline/peralkaline igneous Rocks. In: Verplanck, P.L., Hitzman, M.W. (Eds.), Rare Earth and Critical Elements in Ore Deposits, Rev. Econ. Geol., 18, pp. 33–54. https://doi.org/10.5382/Rev.18.02.

Eby, G.N., 1992. Chemical subdivision of the A-type granitoids: petrogenetic and tectonic implications. Geology 20, 641–644. https://doi.org/10.1130/00917613(1992)020<0641:CSOTAT>2.3.CO;2.

Elo, S., 1997. Interpretations of the gravity anomaly map of Finland. Geophysica 33, 51–80.

Ersoy, E.Y., Helvacı, C., Palmer, M.R., 2010. Mantle source characteristics and melting models for the early-middle Miocene mafic volcanism in Western Anatolia: implications for enrichment processes of mantle lithosphere and origin of K-rich volcanism in post-collisional settings. J. Volcanol. Geotherm. Res. 198, 112–128. https://doi.org/10.1016/j.jvolgeores.2010.08.014.

Ewart, A., Griffin, W.L., 1994. Application of proton-microprobe data to trace-element partitioning in volcanic rocks. Chem. Geol. 117, 251–284. https://doi.org/10.1016/0009-2541(94)90131-7.

Farmer, G.L., 2003. Continental basaltic rocks. In: Rudnick, R.L. (Ed.), The Crust. Treatise on Geochemistry, Volume 3. Elsevier-Pergamon, Oxford, pp. 85–121. https://doi.org/10.1016/B0-08-043751-6/03019-X.

Floyd, P.A., Winchester, J.A., 1975. Magma type and tectonic setting discrimination using immobile elements. Earth Planet. Sci. Lett. 27, 211–218. https://doi.org/10.1016/0012-821X(75)90031-X.

Frost, B.R., Frost, C.D., 2008. A geochemical classification for feldspathic igneous rocks. J. Petrol. 49, 1955–1969. https://doi.org/10.1093/petrology/egn054.

Frost, C.D., Frost, B.R., 2011. On ferroan (A-type) granitoids: their compositional variability and modes of origin. J. Petrol. 52, 39–53. https://doi.org/10.1093/petrology/egq070.

Ghiorso, M.S., Gualda, G.A.R., 2015. An H_2O-CO_2 mixed fluid saturation model compatible with rhyolite-MELTS. Contrib. Mineral. Petrol. 169, 53. https://doi.org/10.1007/s00410-015-1141-8.

Ghiorso, M.S., Sack, R.O., 1995. Chemical mass transfer in magmatic processes. IV. A revised and internally consistent thermodynamic model for the interpolation and extrapolation of liquid-solid equilibria in magmatic systems at elevated temperatures and pressures. Contrib. Mineral. Petrol. 119, 197–212. https://doi.org/10.1007/BF00307281.

Grebennikov, A.V., 2014. A-type granites and related rocks: petrogenesis and classification. Rus. Geol. Geophys. 55, 1074–1086. https://doi.org/10.1016/j.rgg.2014.08.003.

Gualda, G.A.R., Ghiorso, M.S., Lemons, R.V., Carley, T.L., 2012. Rhyolite-MELTS: a modified calibration of MELTS optimized for silica-rich, fluid-bearing magmatic systems. J. Petrol. 53, 875–890. https://doi.org/10.1093/petrology/egr080.

Hanski, E.J., 2013. Evolution of the paleoproterozoic (2.50−1.95 Ga) non-orogenic magmatism in the eastern part of the fennoscandian shield. In: Melezhik, V.A., Prave, A.R., Hanski, E.J., Fallick, A.E., Lepland, A., Kump, L.R., Strauss, H. (Eds.), Reading the Archive of Earth'S Oxygenation, Volume 1, The Palaeoproterozoic of Fennoscandia as Context for the Fennoscandian Arctic Russia – Drilling Early Earth Project. Springer-Verlag, Berlin, Heidelberg, pp. 179–244. https://doi.org/10.1007/978-3-642-29682-6_6.

Hanski, E.J., Melezhik, V.A., 2013a. Litho- and chronostratigraphy of the palaeoproterozoic Karelian formations. In: Melezhik, V.A., Prave, A.R., Hanski, E.J., Fallick, A.E., Lepland, A., Kump, L.R., Strauss, H. (Eds.), Reading the Archive of Earth'S Oxygenation, Volume 1, The Palaeoproterozoic of Fennoscandia as Context for the Fennoscandian Arctic Russia – Drilling Early Earth Project. Springer-Verlag, Berlin, Heidelberg, pp. 39–110. https://doi.org/10.1007/978-3-642-29682-6_4.

Hanski, E.J., Melezhik, V.A., 2013b. Palaeotectonic and palaeogeographic evolution of fennoscandia in the early palaeoproterozoic. In: Melezhik, V.A., Prave, A.R., Hanski, E.J., Fallick, A.E., Lepland, A., Kump, L.R., Strauss, H. (Eds.), Eds.), Reading the Archive of Earth'S Oxygenation, Volume 1, The Palaeoproterozoic of Fennoscandia as Context for the Fennoscandian Arctic Russia – Drilling Early Earth Project. Springer-Verlag, Berlin, Heidelberg, pp. 111–178. https://doi.org/10.1007/978-3-642-29682-6_5.

Heinonen, J.S., Luttinen, A.V., Bohrson, W.A., 2016. Enriched continental flood basalts from depleted mantle melts: modeling the lithospheric contamination of Karoo lavas from Antarctica. Contrib. Mineral. Petrol. 171 (9) https://doi.org/10.1007/s00410-015-1214-8.

Heinonen, J.S., Luttinen, A.V., Whitehouse, M.J., 2018. Enrichment of ^{18}O in the mantle sources of the Antarctic portion of the Karoo large igneous province. Contrib. Mineral. Petrol. 173, 21. https://doi.org/10.1007/s00410-018-1447-4.

Heinonen, J.S., Bohrson, W.A., Spera, F.J., Brown, G.A., Scruggs, M.A., Adams, J.V., 2020. Diagnosing open-system magmatic processes using the Magma Chamber Simulator (MCS): part II—trace elements and isotopes. Contrib. Mineral. Petrol. 175, 105. https://doi.org/10.1007/s00410-020-01718-9.

Huhma, H., Kontinen, A., Mikkola, P., Halkoaho, T., Hokkanen, T., Hölttä, P., Juopperi, H., Konnunaho, J., Luukkonen, E., Mutanen, T., Peltonen, P., Pietikäinen, K., Pulkkinen, A., 2012. Nd isotopic evidence for Archaean crustal growth in Finland. Geol. Surv. Finl., Spec. Pap. 54, 176–213.

Huhma, H., Hanski, E., Kontinen, A., Vuollo, J., Mänttäri, I., Lahaye, Y., 2018. Sm–Nd and U–Pb isotope geochemistry of the Paleoproterozoic mafic magmatism in eastern and northern Finland. Geol. Surv. Finl., Bull. 405.

Iljina, M., Hanski, E., 2005. Layered mafic intrusions of the Tornio-näränkävaara belt. In: Lehtinen, M., Nurmi, P., Rämö, O.T. (Eds.), Precambrian Bedrock of Finland – Key to the Evolution of the Fennoscandian Shield. Elsevier Science B.V, Amsterdam, pp. 103–138. https://doi.org/10.1016/S0166-2635(05)80004-0.

Jeffery, J., Gertisser, R., 2018. Peralkaline felsic magmatism of the Atlantic islands. Front. Earth Sci. 6, 145. https://doi.org/10.3389/feart.2018.00145.

Kärenlampi, K., Kontinen, A., Huhma, H., Hanski, E., 2019. Geology, geochronology and geochemistry of the 2.05 Ga gneissic A1-type granites and related intermediate rocks in central Finland: implication for the tectonic evolution of the Karelia craton margin. Bull. Geol. Soc. Finl. 91, 35–73. https://doi.org/10.17741/bgsf/91.1.002.

Kärenlampi, K., Kontinen, A., Hanski, E., Huhma, H., Lahaye, Y., Krause, J., Heinig, T., 2020. Age and origin of the Nb-Zr-REE mineralization in the Paleoproterozoic A1-type granitoids at Otanmäki, central Finland. Bull. Geol. Soc. Finl. 92, 39–71. https://doi.org/10.17741/bgsf/92.1.003.

Kontinen, A., Paavola, J., 2006. A preliminary model of the crustal structure of the Eastern Finland Archaean Complex between Vartius and Vieremä, based on constraints from surface geology and FIRE 1 seismic survey. Geol. Surv. Finl., Spec. Pap. 43, 223–240.

Korja, A., Lahtinen, R., Heikkinen, P., Kukkonen, I.T., FIRE working Group, 2006. A geological interpretation of the upper crust along FIRE 1. Geol. Surv. Finl., Spec. Pap. 43, 45–76.

Kozlovskaya, E., Yliniemi, J., 1999. Deep structure of the Earth's crust along the SVEKA profile and its extention to the north-east. Geophysica 35, 111–123.

Krienitz, M.-S., Haase, K.M., Mezger, K., Shaikh-Mashail, M.A., 2007. Magma genesis and mantle dynamics at the harrat ash shamah volcanic field (Southern Syria). J. Petrol. 48, 1513–1542. https://doi.org/10.1093/petrology/egm028.

Lahtinen, R., Huhma, H., Lahaye, Y., Kousa, J., Luukas, J., 2015. Archean–proterozoic collision boundary in central Fennoscandia: revisited. Precambrian Res. 261, 127–165. https://doi.org/10.1016/j.precamres.2015.02.012.

Luttinen, A.V., 2018. Bilateral geochemical asymmetry in the Karoo large igneous province. Sci. Rep. 8 (5223) https://doi.org/10.1038/s41598-018-23661-.

Mahood, G., Hildreth, W., 1983. Large partition coefficients for trace elements in high-silica rhyolites. Geochim. Cosmochim. Acta 47, 11–30. https://doi.org/10.1016/0016-7037(83)90087-X.

Meade, F.C., Troll, V.T., Ellam, R.M., Freda, C., Font, L., Donaldson, C.H., Klonowska, I., 2014. Bimodal magmatism produced by progressively inhibited crustal assimilation. Nat. Commun. 5, 4199. https://doi.org/10.1038/ncomms5199.

Meshesha, D., Shinjo, R., 2007. Crustal contamination and diversity of magma sources in the northwestern Ethiopian volcanic province. J. Miner. Petrol. Sci. 102, 272–290. https://doi.org/10.2465/jmps.061129.

Middlemost, E.A.K., 1994. Naming materials in the magma/igneous rock system. Earth-Sci. Rev. 37, 215–224. https://doi.org/10.1016/0012-8252(94)90029-9.

Mikkola, P., 2011. The Prehistory of Suomussalmi, Eastern Finland; the First Billion Years As Revealed by Isotopes and the Composition of Granitoid Suites. Academic Dissertation. University of Helsinki, p. 24.

Mourtada-Bonnefoi, C.C., Provost, A., Albarède, F., 1999. Thermochemical dynamics of magma chambers: a simple model. J. Geophys. Res. 104, 7103–7115. https://doi.org/10.1029/1998JB900112.

Mücke, A., 2003. Fayalite, pyroxene, amphibole, annite and their decay products in mafic clots within Younger Granites of Nigeria: petrography, mineral chemistry and genetic implications. J. Afr. Earth Sci. 36, 55–71. https://doi.org/10.1016/S0899-5362(03)00015-0.

Nash, W.P., Crecraft, H.R., 1985. Partition coefficients for trace elements in silicic magmas. Geochim. Cosmochim. Acta 49, 2309–2322. https://doi.org/10.1016/0016-7037(85)90231-5.

Nielsen, R.L., Beard, J.S., 2000. Magnetite–melt HFSE partitioning. Chem. Geol. 164, 21–34. https://doi.org/10.1016/S0009-2541(99)00139-4.

Nironen, M., 2005. Proterozoic orogenic granitoid rocks. In: Lehtinen, M., Nurmi, P.A., Rämö, O.T. (Eds.), The Precambrian Geology of Finland – Key to the Evolution of the Fennoscandian Shield. Elsevier Science B.V., Amsterdam, pp. 443–479. https://doi.org/10.1016/S0166-2635(05)80011-8.

Patiño Douce, A., 1997. Generation of metaluminous A-type granites by low pressure melting of calc-alkaline granitoids. Geology 25, 743–746. https://doi.org/10.1130/00917613(1997)025<0743:GOMATG>2.3.CO;2.

Pearce, J.A., 2008. Geochemical fingerprinting of oceanic basalts with applications to ophiolite classification and the search for Archean oceanic crust. Lithos 100, 14–48. https://doi.org/10.1016/j.lithos.2007.06.016.

Pearce, J.A., Harris, N.B.W., Tindle, A.G., 1984. Trace element discrimination diagrams for the tectonic interpretation of granitic rocks. J. Petrol. 25, 956–983. https://doi.org/10.1093/petrology/25.4.956.

Peltonen, P., Kontinen, A., 2004. The jormua ophiolite: a mafic-ultramafic complex from an ancient ocean-continent transition zone. In: Kusky, T.M. (Ed.), Precambrian Ophiolites and Related Rocks. Elsevier B.V., Amsterdam, pp. 35–71. https://doi.org/10.1016/S0166-2635(04)13001-6.

Petrone, C.M., Braschi, E., Francalanci, L., Casalini, M., Tommasini, S., 2018. Rapid mixing and short storage timescale in the magma dynamics of a steady-state volcano. Earth Planet. Sci. Lett. 492, 206–221. https://doi.org/10.1016/j.epsl.2018.03.055.

Prowatke, S., Klemme, S., 2006. Trace element partitioning between apatite and silicate melts. Geochim. Cosmochim. Acta 70, 4513–4527. https://doi.org/10.1016/j.gca.2006.06.162.

Rämö, O.T., Haapala, I., Rämö, O.T., 2005. Rapakivi granites. In: Lehtinen, M., Nurmi, P. A. (Eds.), Eds.), Precambrian Geology of Finland Key to the Evolution of the Fennoscandian Shield. Elsevier Science B.V., Amsterdam, pp. 533–562. https://doi.org/10.1016/S0166-2635(05)80013-1.

Ranta, J.-P., Lauri, L., Hanski, E., Huhma, H., Lahaye, Y., Vanhanen, E., 2015. U–Pb and Sm–Nd isotopic constraints on the evolution of the Paleoproterozoic Peräpohja Belt,

northern Finland. Precambrian Res. 266, 246–259. https://doi.org/10.1016/j.precamres.2015.05.018.
Rasilainen, K., Lahtinen, R., Bornhorst, T.J., 2007. The rock geochemical database of finland manual. Geol. Surv. Finl., Rep. Invest. 164, 38.
Riishuus, M.S., Peate, D.W., Tegner, C., Wilson, J.R., Brooks, C.K., 2008. Petrogenesis of cogenetic silica-oversaturated and -undersaturated syenites by periodic recharge in a crustally contaminated magma chamber: the Kangerlussuaq intrusion, East Greenland. J. Petrol. 49, 493–522. https://doi.org/10.1093/petrology/egm090.
Rogers, N.W., Hawkesworth, C.J., Mattey, D.P., Harmon, R.S., 1987. Sediment subduction and the source of potassium in orogenic leucitites. Geology 15, 451–453. https://doi.org/10.1130/0091-7613(1987)15<451:SSATSO>2.0.CO;2.
Rudnick, R.L., Gao, S., 2003. Composition of the continental crust. In: Rudnick, R.L. (Ed.), The Crust. Treatise on Geochemistry, Vol. 3. Elsevier-Pergamon, Oxford, pp. 1–64.
Shand, S.J., 1943. Eruptive Rocks. Their Genesis Composition, Classification, and Their Relation to Ore-deposits With a Chapter on Meteorites. John Wiley & Sons, New York.
Shellnut, J.G., 2014. The Emeishan large igneous province: a synthesis. Geosci. Front. 5, 369–394. https://doi.org/10.1016/j.gsf.2013.07.003.
Shellnut, J.G., Zhou, M.-F., 2007. Permian peralkaline, peraluminous and metaluminous A-type granites in the Panxi district, SW China: their relationship to the Emeishan mantle plume. Chem. Geol. 243, 286–316. https://doi.org/10.1016/j.chemgeo.2007.05.022.
Shellnutt, J.G., Dostal, J., 2020. Derivation of the Early Carboniferous Wedgeport pluton by crystal fractionation of a mafic parental magma: a rare case of an A-type granite within the Meguma terrane (Nova Scotia). Geol. Mag. 157, 248–262. https://doi.org/10.1017/S0016756819000694.
Shellnutt, J.G., Wang, K.-L., Zellmer, G.F., Iizuka, Y., Jahn, B.-M., Pang, K.-N., Qi, L., Zhou, M.-F., 2011. Three Fe-Ti oxide ore-bearing gabbro-granitoid complexes in the Panxi region of the Emeishan large igneous province, SW China. Am. J. Sci. 311, 773–812. https://doi.org/10.2475/09.2011.02.
Simons, K., Dixon, J., Schilling, J.G., Kingsley, R., Poreda, R., 2002. Volatiles in basaltic glasses from the Easter-Salas y Gomez Seamount Chain and Easter Microplate: implications for geochemical cycling of volatile elements. Geochem. Geophys. Geosyst. 3, 1–29. https://doi.org/10.1029/2001GC000173.
Sisson, T.W., Bacon, C.R., 1992. Garnet high-silica rhyolite trace-element partition-coefficients measured by ion microprobe. Geochim. Cosmochim. Acta 56, 2133–2136. https://doi.org/10.1016/0016-7037(92)90336-H.
Smith, D.R., Noblett, J., Wobus, R.A., Unruh, D., Douglass, J., Beane, R., Davis, C., Goldman, S., Kay, G., Gustavson, B., Saltoun, B., Stewart, J., 1999. Petrology and geochemistry of late-stage intrusions of the A-type, mid-Proterozoic Pikes Peak batholith (Central Colorado, USA): implications for petrogenetic models. Precambrian Res. 98, 271–305. https://doi.org/10.1016/S0301-9268(99)00049-2.
Spandler, C., Hammerli, J., Yaxley, G.M., 2017. An experimental study of trace element distribution during partial melting of mantle heterogeneities. Chem. Geol. 462, 74–87. https://doi.org/10.1016/j.chemgeo.2017.05.002.
Spera, F.J., Bohrson, W.A., Till, C.B., Ghiorso, M.S., 2007. Partitioning of trace elements among coexisting crystals, melt and supercritical fluid during isobaric fractional crystallization and fractional melting. Am. Mineral. 92, 1881–1898. https://doi.org/10.2138/am.2007.2326.
Sun, S.-S., McDonough, W.F., 1989. Chemical and isotopic systematics of oceanic basalts: implications for mantle composition and processes. Geol. Soc. Lond., Spec. Publ. 42, 313–345. https://doi.org/10.1144/GSL.SP.1989.042.01.19.
Tommasini, S., Poli, G., Manetti, P., Conticelli, S., 1994. Oligo-Miocene A-type granites and granophyres from Yemen: isotopic and trace element constraints bearing on their genesis. Eur. J. Miner. 6, 571–590.
Ushioda, M., Takahashi, E., Hamada, M., Suzuki, T., 2014. Water content in arc basaltic magma in the Northeast Japan and Izu arcs: an estimate from Ca/Na partitioning between plagioclase and melt. Earth Planets Space 66, 127. https://doi.org/10.1186/1880-5981-66-127.
van Westrenen, W., Blundy, J., Wood, B., 1999. Crystal chemical controls on trace element partitioning between garnet and anhydrous silicate melt. Am. Mineral. 84, 838–847. https://doi.org/10.2138/am-1999-5-617.
Vilalva, F.C.J., Vlach, S.R.F., 2014. Geology, petrography and geochemistry of the A-type granites from the Morro Redondo Complex (PR-SC), southern Brazil, Graciosa Province. Earth Sci. 86, 85–116. https://doi.org/10.1590/0001-37652014108312.
Vuollo, J., Huhma, H., 2005. Palaeoproterozoic mafic dykes in NE Finland. In: Lehtinen, M., Nurmi, P.A., Rämö, O.T. (Eds.), Eds.), Precambrian Geology of Finland – Key to the Evolution of the Fennoscandian Shield. Elsevier Science B.V., Amsterdam, pp. 193–235. https://doi.org/10.1016/S0166-2635(05)80006-4.
Wallace, P.J., 1998. Water and partial melting in mantle plumes: inferences from the dissolved H2O concentrations of Hawaiian basaltic magmas. Geophys. Res. Lett. 25, 3639–3642. https://doi.org/10.1029/98GL02805.
Wang, X.-C., Wilde, S.A., Xu, B., Pang, C.J., 2016. Origin of arc-like continental basalts: implications for deep-Earth fluid cycling and tectonic discrimination. Lithos 261, 5–45. https://doi.org/10.1016/j.lithos.2015.12.014.
Weis, F.A., Skogby, H., Troll, V.R., Deegan, F.M., Dahren, B., 2015. Magmatic water contents determined through clinopyroxene: examples from the Western Canary Islands. Spain. Geochem. Geophys. Geosyst. 16, 2127–2146. https://doi.org/10.1002/2015GC005800.
Whalen, J.B., Currie, K.L., Chappell, B.W., 1987. A-type granites: geochemical characteristics, discrimination and petrogenesis. Contrib. Mineral. Petrol. 95, 407–419. https://doi.org/10.1007/BF00402202.
Whitehouse, M.J., Windley, B.F., Stoeser, D.B., Ba-Bttat, M.A.O., Haider, A., 2001. Precambrian basement character of Yemen and correlations with Saudi Arabia and Somalia. Precambrian Res. 105, 357–369. https://doi.org/10.1016/S0301-9268(00)00120-0.